Switching from Metal- to Ligand-Based Oxidation in Cobalt Complexes with Redox-Active Bisguanidine Ligands

Lukas Lohmeyer,[a] Elisabeth Kaifer,[a] Markus Enders,[a] and Hans-Jörg Himmel*[a]

Abstract: The control of the redox reactivity, magnetic and optical properties of the different redox states of complexes with redox-active ligands permits their rational use in catalysis and materials science. The redox-chemistry of octahedrally coordinated high-spin Co^{II} complexes (three unpaired electrons) with one redox-active bisguanidine ligand and two acetylacetonato (acac) co-ligands is completely changed by replacing the acac by hexafluoro-acetylacetonato (hfacac) co-ligands. The first one-electron oxidation is metal-centered in the case of the complexes with acac co-ligands, giving diamagnetic Co^{III} complexes. By contrast, in the case of the less Lewis-basic hfacac co-ligands, the first one-electron oxidation becomes ligand-centered, leading to high-spin Co^{II} complexes with a radical monocationic guanidine ligand unit (four unpaired electrons). Ferromagnetic coupling between the spins on the metal and the organic radical in solution is evidenced by temperature-dependent paramagnetic NMR studies, allowing to estimate the isotropic exchange coupling constant in solution. Second one-electron oxidation leads to high-spin Co^{II} complexes with dicationic guanidine ligand units (three unpaired electrons) in the presence of hfacac co-ligands, but to low-spin Co^{III} complexes with radical mono-cationic, peralkylated guanidine ligand (one unpaired electron) in the presence of acac co-ligands. The analysis of the electronic structures is complemented by quantum-chemical calculations on the spin density distributions and relative energies of the possible redox isomers.

Introduction

The integration of redox-active ligands in molecular coordination compounds brings about new attractive prospects in catalysis and materials design.[1–8] In particular, cobalt complexes were intensively studied, due to the massive change in the magnetic and/or optical properties that accompany the transition from high-spin Co^{II} (three unpaired electrons at the metal) to low-spin Co^{III} (no unpaired electron at the metal). In combination with redox-active ligands, intriguing electronic structures and properties result.[9–14] The majority of work uses oxolene-type ligands, for example o-quinones, as redox-active ligands in cobalt complexes. Such complexes could show valence tautomerism (VT, reversible equilibria between two or more redox isomers) in solution and/or in the solid state.[15–18] Complexes were synthesized in which light could be used to switch between two redox isomers having very different electronic structures and magnetic properties (LIESST and reverse-LIESST effect).[19–24] Furthermore, pressure could trigger

conversion between two redox isomers, due to the structural changes upon transition from high-spin Co^{II} with large metal-ligand distances to low-spin Co^{III} with short metal-ligand distances.[25] VT could induce a variety of macroscopic phenomena, including unusual crystal-melt phase transitions.[26] Intramolecular electron transfer (IET) processes were also observed upon oxidation or reduction of a complex with redox-active ligands. Hence, dinuclear cobalt complexes with bridging tetraoxolene ligands were the first compounds showing redox-induced intramolecular electron transfer (RIET), leading to the reduction of the metal atom upon overall oxidation of the complex.[27–29] Recently, it has been shown that the additional coordination of a ligand could trigger spin-flip or metal-to ligand single-electron transfer in cobalt complexes with a dipyrrin-biphenol ligand.[30]

Redox-active guanidines, comprising guanidino-functionalized aromatics (GFAs), were established by our group as a new class of versatile redox-active ligands.[31–33] IET in mono- or dinuclear copper complexes with a GFA ligand could be triggered thermally (VT),[34–37] by redox reactions (RIET),[36] by co-ligand addition[38,39] or substitution,[40] and by metal coordination to a secondary coordination sphere.[41] Also, first applications were disclosed, for example catalytic aerobic phenol homo- and cross-coupling reactions.[42]

In a previous work,[43] we reported the first observation of RIET in cobalt complexes with GFA ligands, triggered in an unprecedented way by interligand hydrogen bonding. We compared the redox-chemistry of cobalt complexes exhibiting one of the three GFAs L1, L2 or L3 (see Figure 1) as redox-active ligands and acetylacetonato (acac) co-ligands. Ligand L3, with partially alkylated guanidino groups, is a hydrogen-bond donor,

[a] L. Lohmeyer, Dr. E. Kaifer, Prof. M. Enders, Prof. H.-J. Himmel
     Inorganic Chemistry
     Ruprecht-Karls University of Heidelberg
     Im Neuenheimer Feld 270, 69120 Heidelberg (Germany)
     E-mail: hans-jorg.himmel@aci.uni-heidelberg.de

Chemistry–A European Journal

Full Paper
doi.org/10.1002/chem.202101364

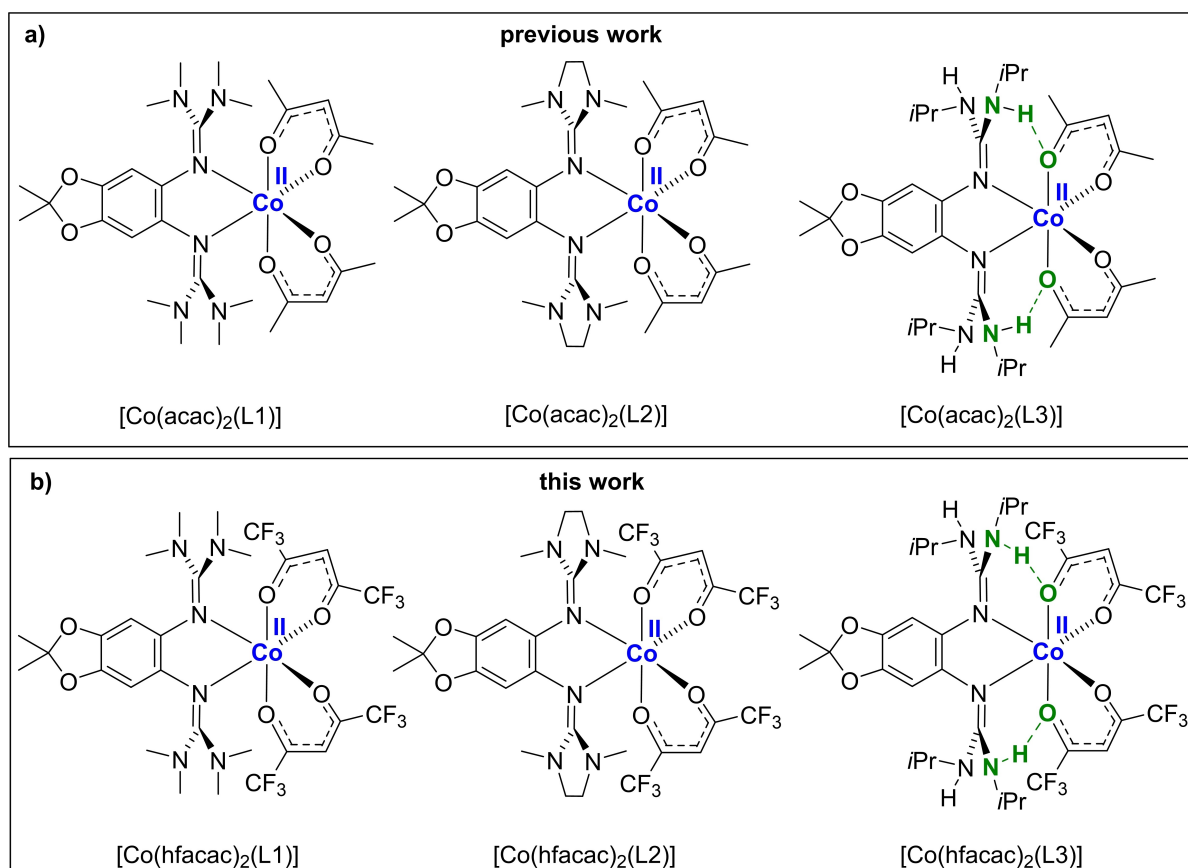**Chemistry Europe**
European Chemical
Societies Publishing

Figure 1. Lewis structures of a) the previously studied Co^{II} complexes with acetylacetonato (acac) and b) the Co^{II} complexes with hexafluoro-acetylacetonato (hfacac) co-ligands studied in this work. One- and two-electron oxidation leads to complexes with oxidized ligand units and/or Co^{III} atoms. L1: 5,6-bis-(*N,N,N′,N′*-tetramethylguanidino)-2,2-dimethyl-[1,3]-benzodioxole; L2: 5,6-bis-(*N,N′*-dimethyl-*N,N′*-ethylene-guanidino)-2,2-dimethyl-[1,3]-benzodioxole; L3: 5,6-bis-(*N,N′*-diisopropyl-guanidino)-2,2-dimethyl-[1,3]-benzodioxole.
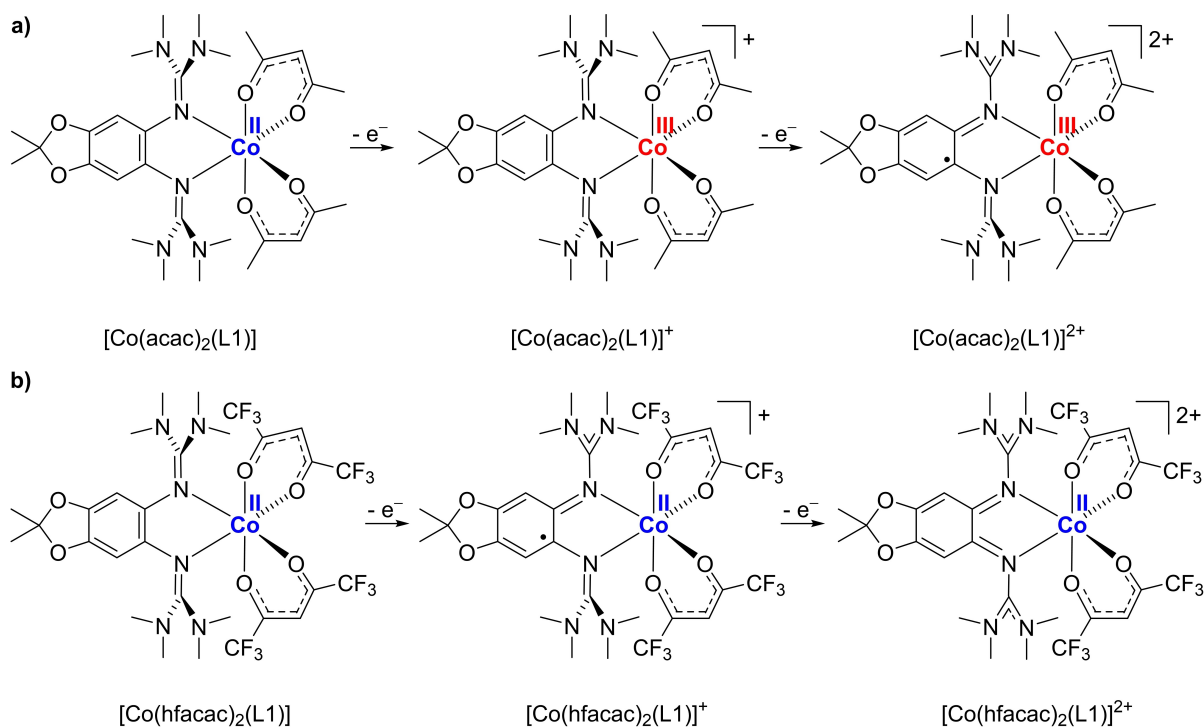
forming interligand hydrogen-bonds with the acac co-ligands. The enforcement of these interligand hydrogen bonds upon oxidation of L3 triggers RIET that otherwise does not occur.[43]

In this work we show that the redox chemistry could be altered by replacing the two acac by hexafluoroacetylacetonato (hfacac) co-ligands. The hfacac co-ligands are less Lewis basic and therefore destabilize Co^{III} with respect to Co^{II}. Consequently, the first oxidation of the neutral Co^{II} complexes changes from a metal-based (for acac co-ligands) to a ligand-based oxidation event. We show that small modifications at the co-ligands allow to control the redox chemistry and electronic structures and properties of the different redox states in a simple way.

Results and Discussion

Reactions between [Co(hfacac)$_2$] and one of the redox-active guanidines L1, L2 or L3 gave the three neutral Co^{II} complexes [Co(hfacac)$_2$(L1)], [Co(hfacac)$_2$(L2)] and [Co(hfacac)$_2$(L3)] in high yield (92–97%). One-electron oxidation of these neutral complexes was carried out with stoichiometric amounts of the ferrocenium (Fc$^+$) salt Fc(PF$_6$) as oxidizing reagent. The three oxidation products [Co(hfacac)$_2$(L1)](PF$_6$), [Co(hfacac)$_2$(L2)](PF$_6$)

and [Co(hfacac)$_2$(L3)](PF$_6$) were isolated in pure form as stable compounds, and it was possible to structurally characterize all of them in the solid state. As detailed in the following, their structures and properties (e.g. magnetism, electronic excitations, redox potentials) are very different to those of the corresponding complexes with acac co-ligands. Hence, the analysis clearly shows that one-electron oxidation occurs at the ligand unit rather than the metal. Consequently, [Co(hfacac)$_2$(L1)](PF$_6$), [Co(hfacac)$_2$(L2)](PF$_6$) and [Co(hfacac)$_2$(L3)](PF$_6$) are high-spin Co^{II} complexes with radical monocationic guanidine ligand (summing up to four unpaired electrons). By contrast, one-electron oxidation of the complexes with the acac co-ligands was shown to be metal-based, leading to diamagnetic Co^{III} complexes with neutral guanidine ligand unit.[43] The second one-electron oxidation leads to high-spin Co^{II} complexes with dicationic guanidine ligand (three unpaired electrons) for complexes with hfacac co-ligands. By contrast, low-spin Co^{III} complexes with radical-monocationic bisguanidine ligand are produced by two-electron oxidation of complexes with acac co-ligands and peralkylated bisguanidine ligands (L1 or L2). Scheme 1 highlights the differences in the electronic structures of the oxidation products for complexes with the redox-active guanidine ligand L1 and either two acac or two

Chemistry–A European Journal

Full Paper
doi.org/10.1002/chem.202101364

Chemistry Europe
European Chemical
Societies Publishing

Scheme 1. Comparison of the Lewis structures for the complexes resulting from stepwise oxidation of a) [Co(acac)$_2$(L1)] and b) [Co(hfacac)$_2$(L1)] in CH$_2$Cl$_2$ solution. Similar results are obtained for complexes with L2.

hfacac co-ligands. The analogue complexes with the redox-active guanidine ligand L2 exhibit similar electronic structures.

In the case of the complexes with ligand L3, intramolecular N–H···O hydrogen bonding between two N–H groups of L3 and an O atom from each of the two acac or hfacac co-ligands affect the electronic structures of the oxidation products. These hydrogen bonds are significantly strengthened upon oxidation of the guanidine ligand. The first two redox processes and the Lewis structures of the oxidation products are sketched in Scheme 2. As highlighted by the box and detailed in a previous work by our group,[43] a RIET process leads to cobalt reduction (Co^{III}→Co^{II}) upon one-electron oxidation of [Co(acac)$_2$(L3)]$^+$ to [Co(acac)$_2$(L3)]$^{2+}$. Therefore, the electronic structures of [Co(hfacac)$_2$(L3)]$^{2+}$ and [Co(acac)$_2$(L3)]$^{2+}$ are similar (Co^{II} complexes with dicationic ligand L3^{2+}).

In the following, we detail the determination of the electronic structures and the properties of the complexes with hfacac co-ligands in three different redox states (neutral, monocationic and dicationic) by a variety of analytical methods, namely cyclic voltammetry (CV), EPR, NMR and UV-vis spectroscopy, structural characterization in the solid state, and quantum-chemical calculations. Due to the special effect of hydrogen-bonding on the electronic structures, the analytical data for complexes with L3 will be discussed separately after the complexes with L1 and L2.

Cyclic voltammetry (CV)

The CV curves recorded for the complexes with hfacac co-ligands in CH$_2$Cl$_2$ solutions show some remarkable differences to those recorded for the complexes with acac co-ligands (Figures 2 and 3 and Table 1). Within the accessible potential window in CH$_2$Cl$_2$, two reversible redox processes are visible for the complexes with hfacac co-ligands, while three redox processes show in the curves recorded for the complexes with
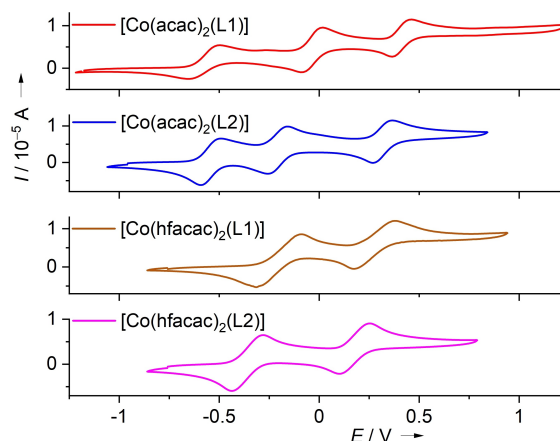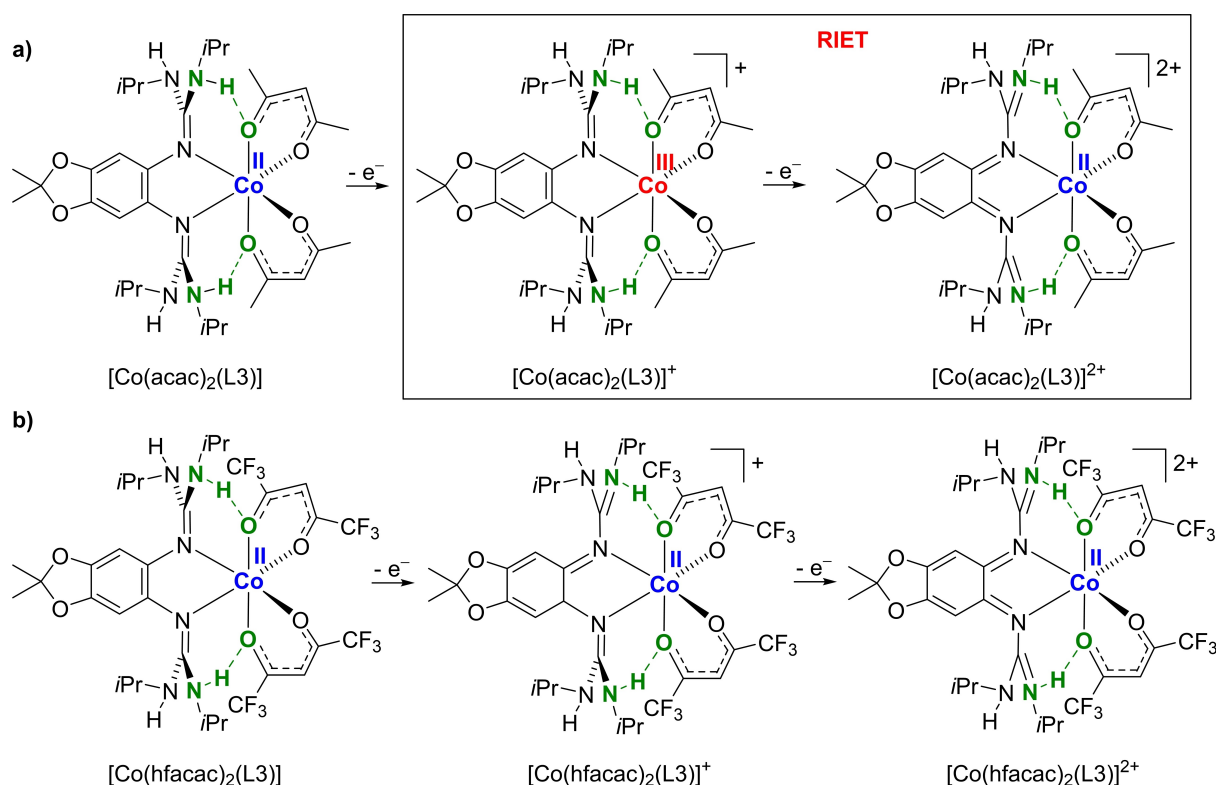

Figure 2. Cyclic voltammograms for the four neutral Co^{II} complexes with L1 and L2 in CH$_2$Cl$_2$ solutions (Ag/AgCl reference electrode, 0.1 M N(^{n}Bu)$_4$PF$_6$ as supporting electrolyte, scan rate 20 mVs^{-1}). The potentials are given vs. the Fc$^+$/Fc redox couple.

Chemistry–A European Journal

Full Paper
doi.org/10.1002/chem.202101364

Chemistry Europe
European Chemical
Societies Publishing

Scheme 2. Comparison of the Lewis structures for the complexes resulting from stepwise oxidation of a) [Co(acac)$_2$(L3)] and b) [Co(hfacac)$_2$(L3)] in CH$_2$Cl$_2$ solutions. a) For the complex with acac co-ligands, the cobalt atom is oxidized to Co^{III} in the first one-electron oxidation step. In the second one-electron oxidation step, the cobalt atom is reduced back to Co^{II} by electron transfer from the ligand L3, being an example for a redox-induced electron transfer (RIET). b) For the analogue complex with hfacac co-ligands, both oxidation steps are ligand-based.
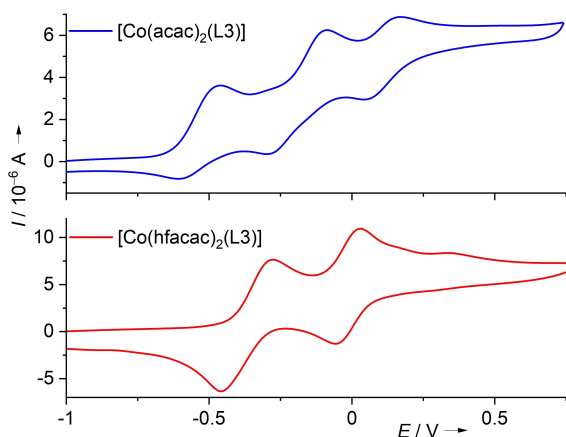

Figure 3. Cyclic voltammograms for the two neutral Co^{II} complexes with L3 in CH$_2$Cl$_2$ solutions (Ag/AgCl reference electrode, 0.1 M N(^{n}Bu)$_4$PF$_6$ as supporting electrolyte, scan rates 20 mV s^{-1} for [Co(acac)$_2$(L3)] and 30 mV s^{-1} for [Co(hfacac)$_2$(L3)]). Potentials given vs. the Fc$^+$/Fc redox couple.

Table 1. Redox potentials (in V vs. Fc$^+$/Fc) for the characterized complexes and the free ligands L1 and L2.

complex	$E_{1/2}(1)/E_{ox}(1)$	$E_{1/2}(2)/E_{ox}(2)$	$E_{1/2}(3)/E_{ox}(3)$
[Co(acac)$_2$(L1)]	−0.56/−0.51	−0.03/0.01	0.41/0.45
[Co(acac)$_2$(L2)]	−0.54/−0.50	−0.21/−0.17	0.32/0.36
[Co(acac)$_2$(L3)]	−0.53/−0.48	−0.19/−0.10	0.11/0.16
[Co(hfacac)$_2$(L1)]	−0.20/−0.09	0.28/0.38	–
[Co(hfacac)$_2$(L2)]	−0.36/−0.29	0.18/0.25	–
[Co(hfacac)$_2$(L3)]	−0.37/−0.28	−0.01/0.03	–
L1	−0.25/−0.19	−0.11/−0.05	–
L2	−0.46/−0.37	−0.33/−0.27	–
L3	–/−0.41	–/0.05	–

The potentials ($E_{1/2}$ values) for the first (one-electron) redox processes in [Co(acac)$_2$(L1)] and [Co(acac)$_2$(L2)], $E_{1/2} = -0.56$ V for [Co(acac)$_2$(L1)]$^+$/[Co(acac)$_2$(L1)] and $E_{1/2} = -0.54$ V for [Co(acac)$_2$(L2)]$^+$/[Co(acac)$_2$(L2)], are lower than the potentials of the free ligands L1 and L2 ($E_{1/2} = -0.25$ V ($E_{ox} = -0.19$ V) for L1$^{·+}$/L1^0 and $E_{1/2} = -0.46$ V ($E_{ox} = -0.37$ V) for L2$^{·+}$/L2^0),[36] clearly showing that they belong to metal-centered redox events.[43] Consequently, one-electron oxidation of the Co^{II} complexes with acac co-ligands leads to Co^{III} complexes with radical monocationic bisguanidine ligand unit. By contrast, the potentials ($E_{1/2}$ values) for the first (one-electron) redox processes in [Co(hfacac)$_2$(L1)] and [Co(hfacac)$_2$(L2)], $E_{1/2} = -0.20$ V ($E_{ox} = -0.09$ V) for [Co(hfacac)$_2$(L1)]$^+$/[Co(hfacac)$_2$(L1)]^0 and $E_{1/2} = -0.36$ V ($E_{ox} = -0.28$ V) for [Co(hfacac)$_2$(L2)]$^+$/[Co(hfacac)$_2$(L2)]^0,

acac co-ligands. Then, the first redox event occurs at significantly higher potential for the complexes with hfacac co-ligands. In the following, we first discuss the CV results for the complexes with L1 and L2 (Figure 2), and then for those with L3 (Figure 3).

Chemistry–A European Journal

Full Paper
doi.org/10.1002/chem.202101364

**Chemistry
Europe**

European Chemical
Societies Publishing

are higher (less negative) than the potentials of the free ligands L1 and L2. Moreover, the $E_{1/2}$ values for the first one-electron oxidation differ significantly for the two complexes [Co(hfacac)$_2$(L1)] and [Co(hfacac)$_2$(L2)]. The potential difference ($\Delta E_{1/2} = 0.16$ V) is similar to that between the free ligands L1 and L2 ($\Delta E_{1/2} = 0.21$ V). Therefore, the CV data are consistent with ligand-centered redox processes for the complexes with hfacac co-ligands, leading to Co^{II} complexes with radical monocationic ligand. The hfacac co-ligand is a weaker Lewis base than acac, stabilizing the Co^{II} redox state with respect to the more Lewis acidic Co^{III} redox state.

The second redox step of the complexes with acac co-ligands (at $E_{1/2} = -0.03$ V for [Co(acac)$_2$(L1)]$^{2+}$/[Co(acac)$_2$(L1)]$^+$ and $E_{1/2} = -0.21$ V for [Co(acac)$_2$(L2)]$^{2+}$/[Co(acac)$_2$(L2)]$^+$) is ligand-centered, resulting in Co^{III} complexes with radical monocationic bisguanidine ligands.[43] Consequently, the potentials for the second redox-step of the complexes with acac co-ligands are not much higher than the potentials for the first redox step of the complexes with hfacac co-ligands; in all cases the ligand is oxidized from the neutral to the radical monocationic redox state.

The second redox processes in the complexes with hfacac co-ligands occur at $E_{1/2} = +0.28$ V ($E_{ox} = +0.38$ V) for the redox couple [Co(hfacac)$_2$(L1)]$^{2+}$/[Co(hfacac)$_2$(L1)]$^+$, and at $E_{1/2} = +0.18$ V ($E_{ox} = +0.25$ V) for the redox couple [Co(hfacac)$_2$(L2)]$^{2+}$/[Co(hfacac)$_2$(L2)]$^+$. Hence, the second one-electron oxidation processes also differ significantly in their $E_{1/2}$ values, by 0.1 V. Moreover, the potentials are higher than those recorded for the redox couples L1^{2+}/L1$^{\cdot+}$ and L2^{2+}/L2$^{\cdot+}$ of the free ligands, $E_{1/2} = -0.11$ V ($E_{ox} = -0.05$ V) for L1^{2+}/L1$^{\cdot+}$, and $E_{1/2} = -0.38$ V ($E_{ox} = -0.27$ V) for L2^{2+}/L2$^{\cdot+}$.[36] On these grounds, they were also assigned to ligand-centered redox processes, leading to Co^{II} complexes with dicationic bisguanidine ligands.

The third oxidation process of the complexes with acac co-ligands, at $E_{1/2} = 0.41$ V for [Co(acac)$_2$(L1)]$^{3+}$/[Co(acac)$_2$(L1)]$^{2+}$ and 0.32 V for [Co(acac)$_2$(L1)]$^{3+}$/[Co(acac)$_2$(L1)]$^{2+}$, produces Co^{III} complexes with dicationic guanidine ligand.[43] The absence of a third redox process for the complexes with hfacac co-ligands within the applied potential window (limited by the solvent) of the CV measurements could be rationalized by the destabilization of the Co^{III} redox state due to the weaker Lewis basicity of the hfacac ligand compared with the acac ligand; therefore the metal-centered Co^{III}/Co^{II} redox process is not observed. Our results on the co-ligand influence on the Co^{III}/Co^{II} redox potential are consistent with previous observations reported for very different cobalt complexes. Hence, for cobalt complexes with two oxolene ligands and a diamine ligand, it has been found that the Co^{II} redox state is stabilized by diamine ligands with a more positive reduction potential, being better π-acceptors, while the Co^{III} redox isomer is favored for less positive reduction potentials.[44] Also, the Co^{III}/Co^{II} transition temperature in cobalt complexes with two oxolene ligands increases for strong N-donor co-ligands.[45]

In summary, the CV data indicate that [Co(hfacac)$_2$(L1)]$^+$ and [Co(hfacac)$_2$(L2)]$^+$ are Co^{II} complexes with radical monocationic bisguanidine ligands, and [Co(hfacac)$_2$(L1)]$^{2+}$ and

[Co(hfacac)$_2$(L2)]$^{2+}$ are Co^{II} complexes with dicationic bisguanidine ligands, in line with the Lewis structures in Scheme 1.

The cyclic voltammograms for [Co(acac)$_2$(L3)] and [Co(hfacac)$_2$(L3)] are compared in Figure 3. In analogy to the results obtained with L1 and L2, three redox waves were obtained for [Co(acac)$_2$(L3)], but only two for [Co(hfacac)$_2$(L3)]. (A tiny feature at higher potentials in the CV of [Co(acac)$_2$(L3)] might be due to a low percentage of redox-induced decomposition.) In the case of [Co(acac)$_2$(L3)], $E_{1/2} = -0.53$ V ($E_{ox} = -0.46$ V) for the first, $E_{1/2} = -0.19$ V ($E_{ox} = -0.09$ V) for the second, and $E_{1/2} = +0.11$ V ($E_{ox} = +0.17$ V) for the third redox process are assigned to the couples [Co(acac)$_2$(L3)]$^+$/[Co(acac)$_2$(L3)]^0, [Co(acac)$_2$(L3)]$^{2+}$/[Co(acac)$_2$(L3)]$^+$ and [Co(acac)$_2$(L3)]$^{3+}$/[Co(acac)$_2$(L3)]$^{2+}$, respectively. As discussed previously,[43] the large potential difference between E_{ox} and E_{red} for the second redox process ([Co(acac)$_2$(L3)]$^{2+}$/[Co(acac)$_2$(L3)]$^+$) arises from the RIET process (see Scheme 2), being accompanied by massive changes in the structural parameters and also in the solvent effect. In the case of [Co(hfacac)$_2$(L3)], one obtains $E_{1/2} = -0.37$ V ($E_{ox} = -0.28$ V) for the first and $E_{1/2} = -0.01$ V ($E_{ox} = +0.03$ V) for the second redox process, assigned to the couples [Co(hfacac)$_2$(L3)]$^+$/[Co(hfacac)$_2$(L3)]^0 and [Co(hfacac)$_2$(L3)]$^{2+}$/[Co(hfacac)$_2$(L3)]$^+$, respectively. The cyclic voltammogram for the free ligand L3 shows irreversible redox processes, hampering a direct comparison with the potentials observed for the complexes.[43] This irreversibility arises from the formation of hydrogen-bonded dimers between the oxidized ligand (being a strong hydrogen-bond donor) and the reduced ligand. The formation, isolation and structural characterization of such hydrogen-bonded aggregates between an oxidized, dicationic GFA and neutral GFAs was reported in detail for 1,2,4,5-tetrakis(diisopropylguanidino)benzene, exhibiting the same partially-alkylated guanidino groups.[46,47] We therefore assigned the two oxidation waves in the cyclic voltammogram of free L3, at $E_{ox} = -0.41$ V and $+0.05$ V, to oxidation of L3 to the (L3^{2+})L3 hydrogen-bonded dimer and to L3^{2+}, respectively.[43] The first of these E_{ox} values (at -0.41 V) is lower than that of [Co(hfacac)$_2$(L3)] ($E_{ox} = -0.28$ V), in line with ligand-centered oxidation to a Co^{II} complex with radical monocationic ligand L3$^{\cdot+}$ (see Scheme 2). By contrast, it is higher than that of [Co(acac)$_2$(L3)] ($E_{ox} = -0.53$ V), in line with cobalt-centered oxidation to a Co^{III} complex with neutral ligand L3 for the complex with acac co-ligands.[43]

EPR and paramagnetic NMR spectroscopy

EPR spectra for the two neutral compounds [Co(hfacac)$_2$(L1)] and [Co(hfacac)$_2$(L2)] are shown in Figure 4, together with those of the corresponding complexes with acac co-ligands. At first glance, the spectrum of [Co(hfacac)$_2$(L1)] looks similar to that of [Co(acac)$_2$(L1)]; with two effective g' values of g'$_\perp$ = 7.10 and g'$_\parallel$ = 2.41. Spin-orbit coupling is large for Co^{II};[48,49] the high orbit contributions lead to high g' values. In the spectrum recorded for [Co(hfacac)$_2$(L2)], the three effective g' factors were obtained (g$_x$ = 6.81, g$_y$ = 2.93, g$_z$ = 1.91). The hyperfine coupling pattern is more complicated for the complexes with hfacac co-ligands.
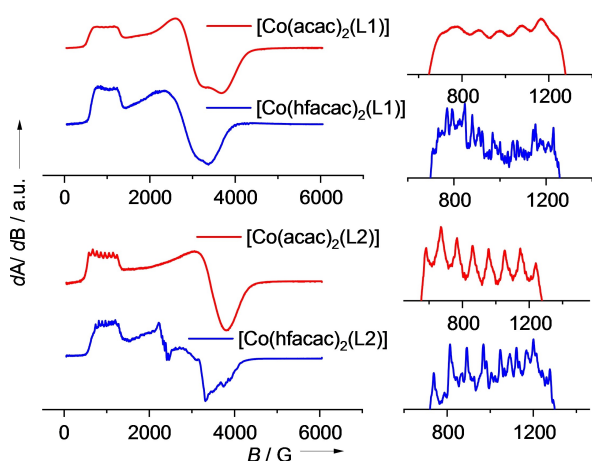
Figure 4. EPR spectra (9.63 GHz, at 6 K in frozen CH_2Cl_2) recorded for the complexes [Co(acac)$_2$(L1)], [Co(hfacac)$_2$(L1)], [Co(acac)$_2$(L2)] and [Co(hfacac)$_2$(L2)].

Coupling to the nuclear spin of the ^{59}Co nucleus (I = 7/2) should produce eight lines, being clearly visible in the spectrum of [Co(acac)$_2$(L2)]. Many more, sharp lines from hyperfine coupling are visible in the spectra recorded for complexes with hfacac co-ligands, due to additional fluorine (and nitrogen) hyperfine splitting.

Interestingly, no clear signals were found in the EPR spectra (both at room temperature and at 6 K) of [Co(hfacac)$_2$(L1)](PF$_6$) and [Co(hfacac)$_2$(L2)](PF$_6$), being Co^{II} complexes with radical monocationic ligands (four unpaired electrons). On the other hand, well resolved signals appeared in the paramagnetic NMR spectra of these compounds. Paramagnetic NMR is well established as powerful tool for the analysis of paramagnetic molecules in solution,[50,51] and has previously been applied by us to study paramagnetic metal-guanidine complexes.[52–54] The ^{13}C NMR spectra of [Co(hfacac)$_2$(L1)](PF$_6$) are shown in Figure 5a. The temperature dependence of the ^{13}C as well as the ^{1}H NMR signals clearly differ from the Curie-Law, mainly due to magnetic coupling between the two spin centers in the molecule. The hyperfine coupling constants A_i as well as the isotropic exchange coupling constant J could be derived by fitting the temperature dependence of each signal. Two hyperfine coupling constants A (A_{Co} and A_{rad}) are expected for each NMR signal due to the different spin values for the two spin centers ($^3/_2$ (Co) and $^1/_2$ (radical ligand), respectively) in [Co-(hfacac)$_2$(L1)](PF$_6$). The fit relies on the formula given below [Eq. (1)];[50c] the resulting fit curves for the temperature dependent signals that could be clearly assigned to specific atoms are shown in Figure 5b.

The derived J value (67 or 71 cm^{-1}, Table 2) confirms a relatively weak ferromagnetic coupling and is supported by the DFT calculations yielding values between 65 cm^{-1} and 130 cm^{-1} depending on the used formula (see Supporting Information for details). The obtained hyperfine coupling constants are in line with the expectations, giving large A_{rad} values for the carbon atoms in the radical ligand and a smaller value for the carbon in the CH group of the hfacac co-ligand (Table 2). The hyperfine coupling to the unpaired electrons located at the Co atom, A_{Co}, is considerably smaller than A_{rad} for all three carbon atoms with the smallest value for the carbon atom of the hfacac ligand. This can be interpreted as a weaker covalency between the hfacac ligand and the Co atom in comparison to the interaction between the bisguanidine ligand and the Co atom.

For the EPR spectrum of complex [Co(hfacac)$_2$(L3)] (Figure 6), g' values of g'$_{||}$ = 6.33 and g'$_\perp$ = 2.79 are obtained. The hyperfine coupling to the nuclear spin of the ^{59}Co nucleus is clearly visible, splitting the first signal into eight lines (coupling constant A = 60 G). However, additional lines appear due to fluorine and nitrogen hyperfine splitting.

Colors and UV-vis spectra

We discuss exemplarily the complexes with ligands L1 and L3. Information about the complexes with ligand L2 are included in the Supporting Information. Figure 7 shows photos of CH_3CN solutions of the complexes [Co(acac)$_2$(L1)](PF$_6$) (with neutral ligand L1), [Co(hfacac)$_2$(L1)](PF$_6$) and [Co(acac)$_2$(L1)](PF$_6$)$_2$ (both with radical monocationic ligand L1$^{·+}$), and [Co(hfacac)$_2$(L1)](SbF$_6$)$_2$ (with dicationic ligand L^{2+}). The green color observed for the solution of [Co(acac)$_2$(L1)](PF$_6$) presumably arises from d–d transitions of the Co^{III} atom. The complexes with radical monocationic ligand L1$^{·+}$, [Co(hfacac)$_2$(L1)](PF$_6$) and [Co(acac)$_2$(L1)](PF$_6$)$_2$, give deep-colored solutions; [Co(hfacac)$_2$(L1)](SbF$_6$)$_2$ with dicationic ligand L1^{2+} leads to orange solutions.

UV-vis spectra were recorded to obtain more detailed information about the electronic excitations (see Figures 8 and 9). In the UV-vis spectra of the neutral complexes with ligand L1 (Figure 8), strong absorptions appeared in the UV region, but only unstructured, weak and extremely broad absorptions in the visible region, assigned to d-d transitions of the Co^{II} atoms. For comparison, the UV-vis spectrum of free, neutral L1 in CH_3CN shows bands at 334 and 300 nm, and that of free, neutral L2 shows bands at 336 and 277 nm.[36]

The visible region was also free of strong bands in the spectra of the monocations [Co(acac)$_2$(L1)]$^+$ or [Co(acac)$_2$(L2)]$^+$,

$$\delta_{Fc,T} = 10^6 \cdot \frac{g_e \beta_e}{3\gamma_i k_B T} \cdot \left(A_{rad} \frac{-\frac{3}{2} e^{\frac{J}{k_B T}} + \frac{15}{2} e^{\frac{3J}{k_B T}}}{3 e^{\frac{J}{k_B T}} + 5 e^{\frac{3J}{k_B T}}} \right.$$
$$\left. + A_{Co} \frac{\frac{15}{2} e^{\frac{J}{k_B T}} + \frac{45}{2} e^{\frac{3J}{k_B T}}}{3 e^{\frac{J}{k_B T}} + 5 e^{\frac{3J}{k_B T}}} \right)$$

(1)

Table 2. Values for the hyperfine coupling constants A_{Co} and A_{rad} and the isotropic exchange coupling constant J from curve fits of the temperature dependence for three signals in the ^{13}C NMR spectra.

signal	A_{rad}/MHz	A_{Co}/MHz	J/cm^{-1}
<u>C</u>H	6.22	−0.16	71
<u>C</u>H	−16.07	3.34	67
<u>C</u>	−8.27	1.43	71

Chemistry–A European Journal

Full Paper
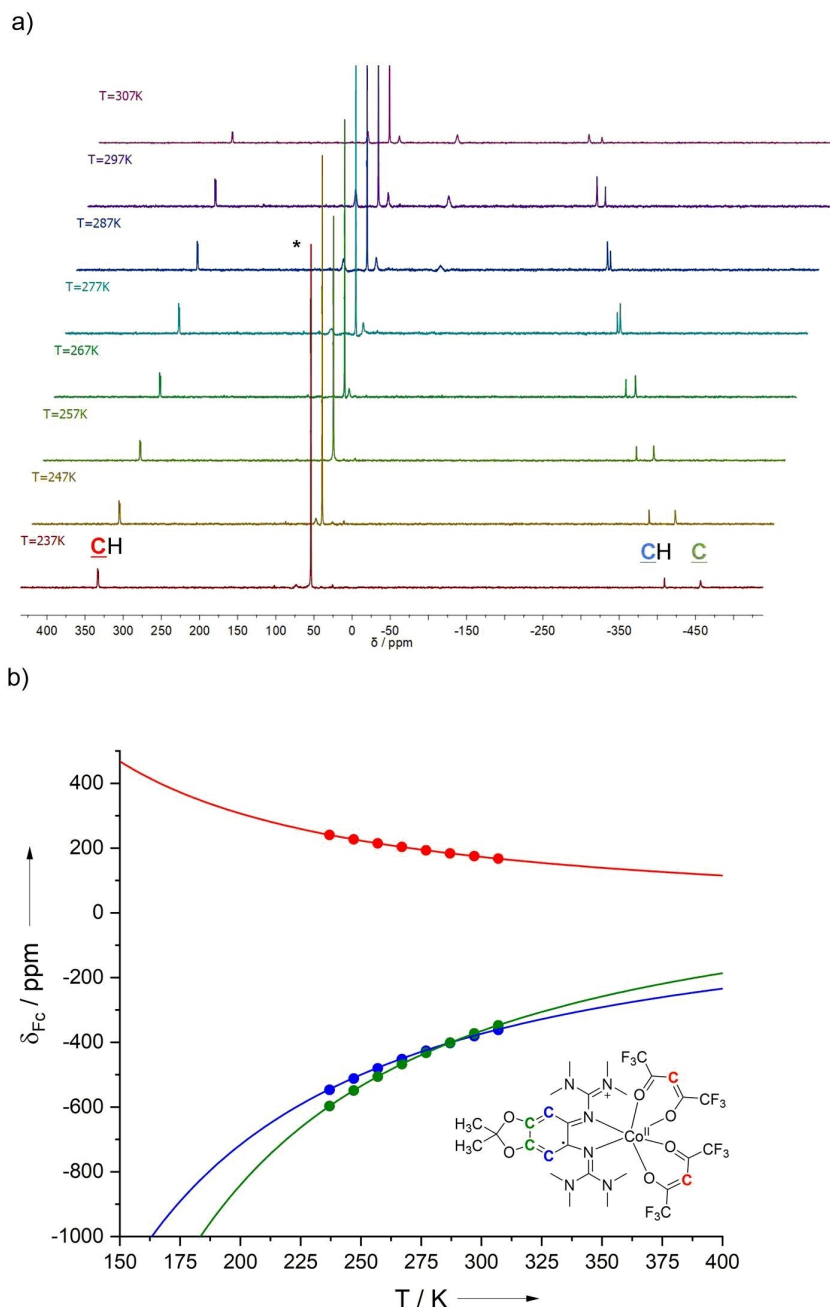doi.org/10.1002/chem.202101364

Chemistry
Europe
European Chemical
Societies Publishing

Figure 5. a) Paramagnetic ^{13}C NMR spectra (CD_2Cl_2) at different temperatures for $[Co(hfacac)_2(L1)](PF_6)$. Solvent signal marked by an asterisk. b) Plot of δ_{FC} versus temperature (T). Experimental data points are shown in the respective color. Curves obtained by fitting the experimental data with Equation (1) is included as solid lines. The fitting procedure relied on a simplex algorithm in which the sum of the root square deviations between experimental and calculated δ_{FC} values is minimized. The fit parameters J, A_{Co} and A_{rad} are collected in Table 2.

arguing for metal-centered oxidation ($Co^{II} \rightarrow Co^{III}$) in line with the results from cyclic voltammetry and EPR spectroscopy.[43] By contrast, a strong band around 370 nm together with a smaller one around 480 nm are present in the UV-vis spectra of the analogue monocationic complexes $[Co(hfacac)_2(L1)]^+$ and $[Co(hfacac)_2(L2)]^+$, indicating ligand-centered oxidation ($L \rightarrow L^{\cdot +}$). For comparison, the free radical monocationic ligand $L1^{\cdot +}$ exhibits a band at 370 nm with a long tail extending into the visible region; a band at ca. 370 nm (with a shoulder around

385 m) is also present for free $L2^{\cdot +}$, and also a broad band in the vis region (with maxima of absorption around 675/733 nm).[36]

Then, the spectra recorded for the dications $[Co(acac)_2 (L1)]^{2+}$ and $[Co(acac)_2(L2)]^{2+}$ in CH_2Cl_2 obtained upon two-electron oxidation contained a band at 364 nm and a broad absorption in the visible region, with absorption maximum at ca. 554 nm for $[Co(acac)_2(L1)]^{2+}$ and 503 nm for $[Co(acac)_2$
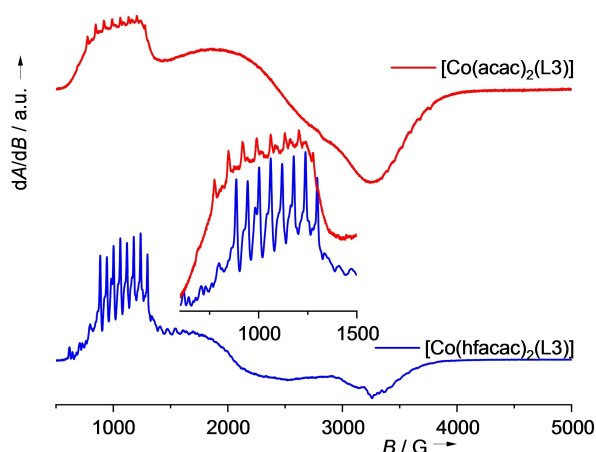
Chemistry–A European Journal

Full Paper
doi.org/10.1002/chem.202101364

Chemistry Europe
European Chemical
Societies Publishing

Figure 6. EPR spectra (9.63 GHz, at 6 K in frozen CH_2Cl_2) recorded for the complexes [Co(acac)$_2$(L3)] and [Co(hfacac)$_2$(L3)] at 6 K.

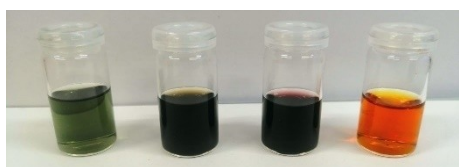**Figure 7.** From left to right: Photos of CH_3CN solutions of the complexes [Co(acac)$_2$(L1)](PF$_6$) (with neutral ligand L1), [Co(hfacac)$_2$(L1)](PF$_6$) and [Co(acac)$_2$(L1)](PF$_6$)$_2$ (both with radical monocationic ligand L$^{·+}$), and [Co(hfacac)$_2$(L1)](SbF$_6$)$_2$ (with dicationic ligand L^{2+}).

(L2)]$^{2+}$, in line with the presence of a Co^{III} complex with radical monocationic ligand.[43]

Due to the higher polarity caused by the introduction of CF$_3$ groups in the co-ligands, the twofold oxidized hfacac-com-

plexes were insoluble in CH_2Cl_2 and were therefore measured in CH_3CN solutions. For the twofold oxidized hfacac-complexes, strong absorptions around 450 nm and 300 nm, matching the bands for the free, twofold oxidized ligand, were found in the UV-vis spectra, arguing for a Co^{II} complex with dicationic ligand unit. For the salts L1(PF$_6$)$_2$ and L2(PF$_6$)$_2$ of the dicationic redox states, also in CH_3CN solution, bands at 450 and 300 nm were observed.[36]

In summary, the UV-vis spectra are in line with the results from cyclic voltammetry and EPR spectroscopy, supporting the Lewis structures shown in Scheme 1.

Bands at 295 and 450 nm in the spectrum of [Co(acac)$_2$(L3)](PF$_6$)$_2$ in CH_2Cl_2 clearly indicate the presence of the dicationic ligand, L3^{2+}, implying the presence of Co^{II}. Similar bands (maxima of absorption at 442 and 306 nm) were found for the analogue complex with hfacac co-ligands in CH_3CN solution (Figure 9). These results strongly suggest that [Co(acac)$_2$(L3)]$^{2+}$ and [Co(acac)$_2$(L3)]$^{2+}$ could both be described as Co^{II} complexes with a dicationic ligand unit, L3^{2+}.

Crystal structures

The solid-state structures of the neutral complexes [Co(hfacac)$_2$(L1)] and [Co(hfacac)$_2$(L2)], as determined by X-ray diffraction (XRD), are visualized in Figure 10a; structural parameters are collected in Tables 3 and 4. In both complexes, the bisguanidine ligand binds with the imino N atoms of the two guanidino groups to the metal, leading to an octahedral coordination of the cobalt atom. The Co–N and Co–O bond lengths measure 2.061(4)/2.093(4) Å and 2.089(4)/2.096(3) Å for [Co(hfacac)$_2$(L1)], and 2.076(2)/2.116(2) Å and 2.091(2)/2.114(2) Å for [Co(hfacac)$_2$(L2)]. The Co–O bond distances between the cobalt atom and the oxygen atoms of the co-ligands are slightly longer for the
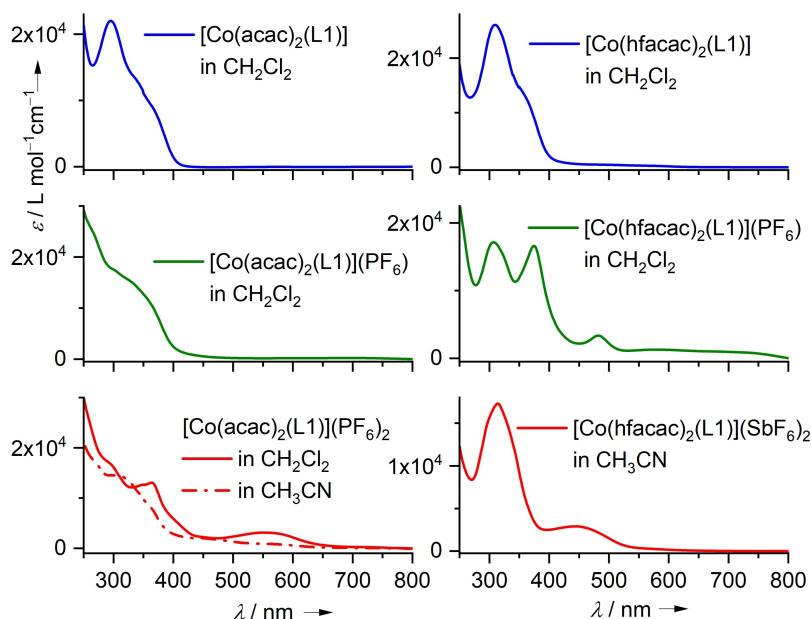

Figure 8. Comparison between the UV-vis spectra recorded for the redox states of the complexes with L1 and acac or hfacac co-ligands.
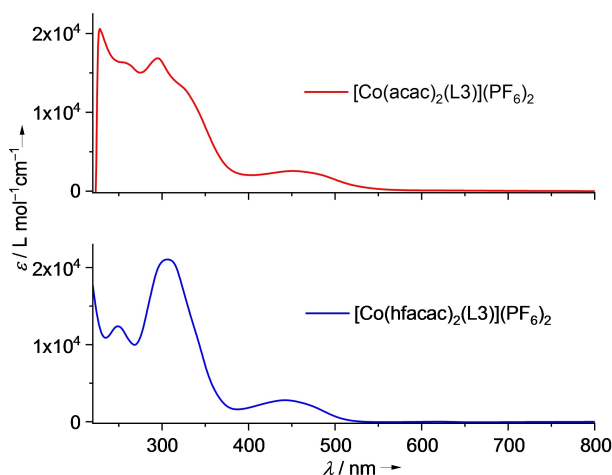
Chem. Eur. J. **2021**, *27*, 11852 – 11867   www.chemeurj.org

11859   © 2021 The Authors. Chemistry - A European Journal published by Wiley-VCH GmbH

Chemistry–A European Journal

Full Paper
doi.org/10.1002/chem.202101364

Chemistry Europe
European Chemical
Societies Publishing

Figure 9. UV-vis spectra of [Co(acac)$_2$(L3)](PF$_6$)$_2$ dissolved in CH$_2$Cl$_2$ and of [Co(hfacac)$_2$(L3)](PF$_6$)$_2$ dissolved in CH$_3$CN.

hfacac ligands compared with the acac ligands (cf. 2.076(2)/ 2.116(2) Å for [Co(acac)$_2$(L2)]), reflecting the poorer Lewis basicity of the hfacac ligand due to the electron-withdrawing CF$_3$ groups. The increase of the N=C bond lengths, from 1.295(1)/1.292(1) Å and 1.293(2)/1.287(2) Å in free L1 and L2, respectively, to 1.418(6)/1.424(6) Å in [Co(hfacac)$_2$(L1)] and

1.325(3)/1.318(3) Å in [Co(hfacac)$_2$(L2)], could be explained by the σ- and π-contributions to the metal-guanidine bonding.[55]

Upon one-electron oxidation of the complexes with hfacac co-ligands (see Figure 10b and Tables 3 and 4), the bond distances within the guanidine ligand unit change significantly. The increase of the C1−C2 bond length from 1.408(3) Å in [Co(hfacac)$_2$(L2)] to 1.466(3) Å in [Co(hfacac)$_2$(L2)]$^+$ and the decrease of the C1−N1 and C2−N4 bond distances clearly signal oxidation of the guanidine ligand unit. Complementary, the bond lengths of the C=N double bonds increase from 1.325(3)/ 1.318(3) Å in [Co(hfacac)$_2$(L2)] to 1.364(3)/1.362(3) Å in [Co(hfacac)$_2$(L2)]$^+$. On the other hand, the Co−O and Co−N bond distances change only slightly, indicating conservation of high-spin Co^{II}. By contrast, these bond distances change significantly upon one-electron oxidation of the complexes with acac co-ligands, indicating Co^{II} to Co^{III} conversion.

The structural changes upon one-electron oxidation of the complex [Co(hfacac)$_2$(L3)] (see Table 5 and the illustration of structures in Figure 11) also indicate ligand-centered oxidation to give the radical monocationic ligand L3$^{\cdot+}$ (e.g. increase of the C1−C2 bond length from 1.400(5) Å to 1.459(6) Å). As expected, the variations in the Co−N and Co−O bond distances are very small, in line with conservation of high-spin Co^{II}. The N···O separation within the N−H···O hydrogen bond is similar in the neutral complexes [Co(acac)$_2$(L3)] and [Co(hfacac)$_2$(L3)]; values of 3.033/2.966 Å and 3.033/2.951 Å, respectively, are

a)

b)
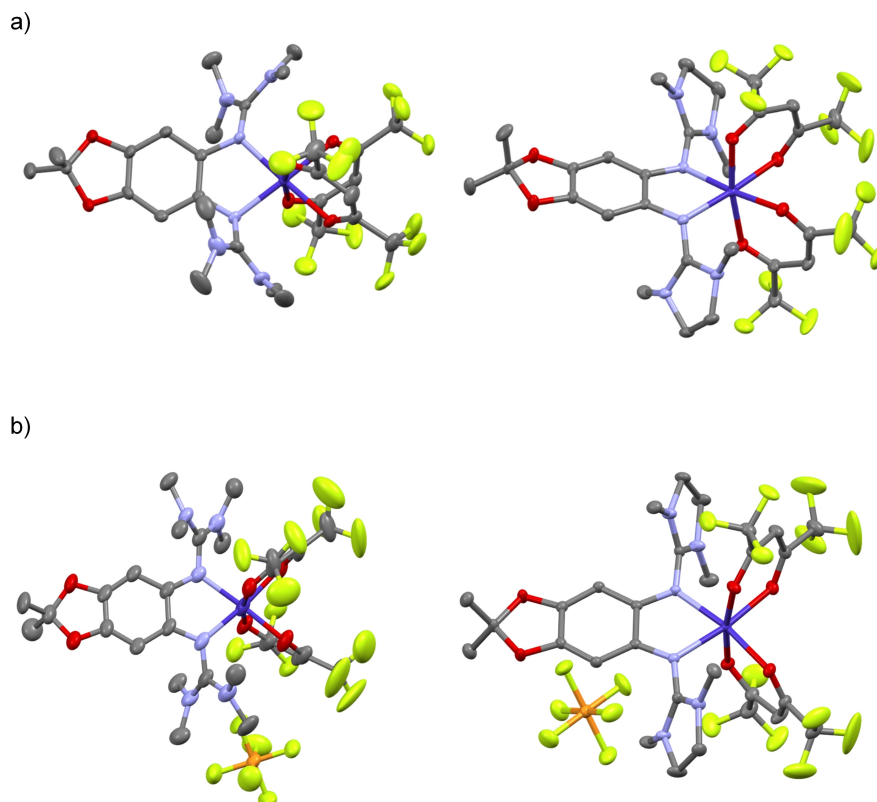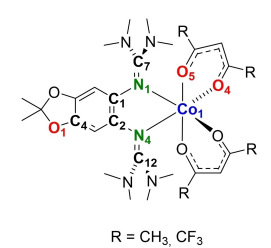
Figure 10. Illustration of the solid-state structures of a) the neutral complexes [Co(hfacac)$_2$(L1)] and [Co(hfacac)$_2$(L2)], and b) the complexes [Co(hfacac)$_2$(L1)](PF$_6$) and [Co(hfacac)$_2$(L2)](PF$_6$) obtained upon one-electron oxidation of the neutral complexes. C−H hydrogens omitted. Displacement ellipsoids drawn at the 50% probability level. Color code: Co blue, O red, C dark grey, F light green.

Chemistry–A European Journal

Full Paper
doi.org/10.1002/chem.202101364

Chemistry
Europe
European Chemical
Societies Publishing

Table 3. Selected bond lengths (in Å) for structurally-characterized cobalt complexes with ligand L1 in the solid state.[56]

parameter	[Co(acac)$_2$(L1)]	[Co(acac)$_2$(L1)](PF$_6$)	[Co(acac)$_2$(L1)](SbF$_6$)$_2$
N1–Co1	2.135(2)	1.960(3)	1.952(2)
N4–Co1	2.149(2)	1.965(3)	1.960(2)
Co1–O5	2.059(1)	1.896(3)	1.896(2)
Co1–O4	2.077(1)	1.888(3)	1.890(2)
C1–N1	1.410(2)	1.404(5)	1.359(4)
C2–N4	1.406(2)	1.424(5)	1.365(4)
N1–C7	1.325(3)	1.347(5)	1.382(4)
N4–C12	1.318(3)	1.342(5)	1.382(4)
C1–C2	1.411(3)	1.405(5)	1.440(4)
C4–O1	1.389(2)	1.383(5)	1.352(4)
parameter	[Co(hfacac)$_2$(L1)]	[Co(hfacac)$_2$(L1)](PF$_6$)	
N1–Co1	2.061(4)	2.088(4)	
N4–Co1	2.093(4)	2.082(4)	
Co1–O5	2.089(4)	2.078(4)	
Co1–O4	2.096(3)	2.072(4)	
C1–N1	1.418(6)	1.346(7)	
C2–N4	1.424(6)	1.366(6)	
N1–C7	1.335(6)	1.372(7)	
N4–C12	1.327(6)	1.379(7)	
C1–C2	1.399(6)	1.445(7)	
C4–O1	1.383(6)	1.347(6)	

R = CH$_3$, CF$_3$

Table 4. Selected bond lengths (in Å) for structurally-characterized cobalt complexes with ligand L2 in the solid state.[56]

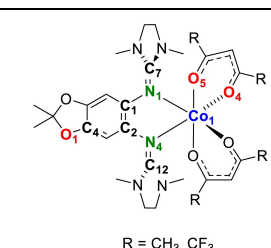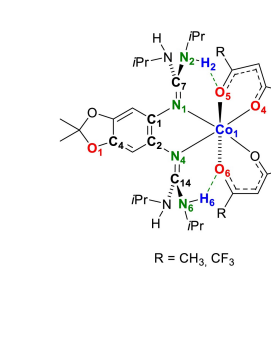| parameter	[Co(acac)$_2$(L2)]	[Co(hfacac)$_2$(L2)]	[Co(hfacac)$_2$(L2)](PF$_6$)
N1–Co1	2.171(2)	2.076(2)	2.087(2)
N4–Co1	2.143(2)	2.116(2)	2.095(2)
Co1–O5	2.071(2)	2.091(2)	2.053(2)
Co1–O4	2.062(2)	2.114(2)	2.102(2)
C1–N1	1.401(3)	1.415(2)	1.349(3)
C2–N4	1.404(3)	1.422(3)	1.359(3)
N1–C7	1.315(3)	1.325(3)	1.364(3)
N4–C12	1.319(3)	1.318(3)	1.362(3)
C1–C2	1.417(3)	1.408(3)	1.466(3)
C4–O1	1.380(3)	1.377(2)	1.352(3)

R = CH$_3$, CF$_3$

Table 5. Selected bond lengths (in Å) for the structurally characterized complexes with L3.[56]

parameter	[Co(acac)$_2$(L3)]	[Co(hfacac)$_2$(L3)]	[Co(hfacac)$_2$(L3)](PF$_6$)
N1–Co	2.161(5)	2.089(3)	2.050(4)
N4–Co	2.138(6)	2.076(3)	2.060(4)
Co1–O4	2.059(6)	2.083(3)	2.112(3)
Co1–O6	2.106(4)	2.103(3)	2.073(3)
C1–N1	1.410(8)	1.411(5)	1.345(5)
C2–N4	1.402(7)	1.358(5)	1.358(5)
N1–C7	1.308(7)	1.319(5)	1.385(6)
N4–C14	1.332(9)	1.314(4)	1.373(5)
C1–C2	1.417(9)	1.400(5)	1.459(6)
C4–O1	1.391(8)	1.385(4)	1.357(5)
H2–O5	2.15(6)	2.33(5)	2.39(5)
H6–O6	2.22(6)	2.22(4)	2.39(5)
N2–O5	2.966(8)	3.030(4)	3.078(4)
N6–O6	3.033(9)	2.951(4)	3.071(5)
∡ N2–H2–O5	156(5)	143(4)	140(4)
∡ N6–H6–O6	154(4)	160(4)	153(4)

R = CH$_3$, CF$_3$

found. Upon oxidation of [Co(hfacac)$_2$(L3)] the N···O separation slightly increases to 3.078/3.071 Å in the radical monocationic complex [Co(hfacac)$_2$(L3)](PF$_6$), presumably due to the changes in the other bond parameters.

The clear dependency of the bond lengths in the bisguanidine ligand on the redox states could be used to establish a "metrical oxidation state", similar to that formulated for amino-phenol- or diazadiene-based ligands.[57,58] Several complexes with redox-active guanidine ligands in different oxidation states are known, but the majority of these complexes contain bridging tetrakisguanidine ligands with a different charge distribution than bisguanidine ligands. Nevertheless, as a start a plot of the C1–N1/C2–N4 and C1–C2 bond lengths as a function of the oxidation state (comprising structures of free
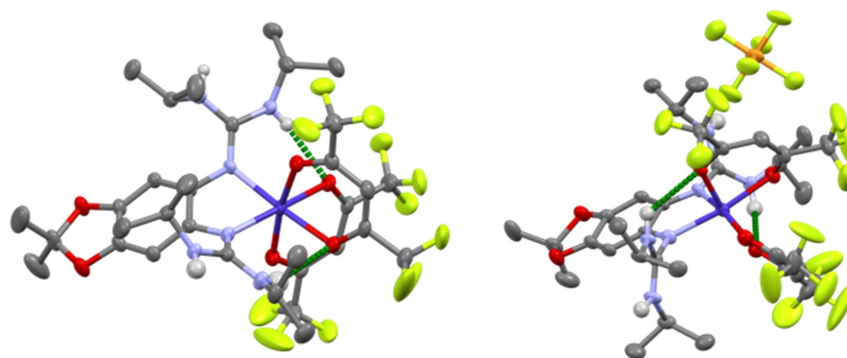
Chemistry–A European Journal

Full Paper
doi.org/10.1002/chem.202101364

**Chemistry
Europe**
European Chemical
Societies Publishing

Figure 11. Visualization of the solid-state structures of [Co(hfacac)$_2$(L3)] and [Co(hfacac)$_2$(L3)](PF$_6$). C–H hydrogens omitted. Displacement ellipsoids drawn at the 50% probability level. Color code: Co blue, O red, C dark grey, N–H hydrogens light grey, F light green.

and coordinated bisguanidine ligands in different redox states) and a linear fit is included in the Supporting Information.

SQUID measurements

We first discuss the magnetometric data of the complexes with L1 or L2, [Co(hfacac)$_2$(L1)](PF$_6$), [Co(hfacac)$_2$(L2)](PF$_6$), [Co(hfacac)$_2$(L1)](SbF$_6$)$_2$ and [Co(hfacac)$_2$(L2)](SbF$_6$)$_2$ (Figure 12). For the monocationic complexes, χT values at 300 K of 3.309 cm^3·K·mol^{-1} {[Co(hfacac)$_2$(L1)](PF$_6$)} and 3.027 cm^3·K·mol^{-1} {[Co(hfacac)$_2$(L2)](PF$_6$)} were measured, indicating a quintet spin state, in line with the other experimental results. Due to an unquenched orbital contribution, the values are higher than the 3.001 cm^3 K mol^{-1} predicted by the Curie law for compounds with S = 2. Below 70 K, χT decreases rapidly to eventually reach values of 0.9210 cm^3·K·mol^{-1} for [Co(hfacac)$_2$(L1)](PF$_6$) and 0.659 cm^3·K·mol^{-1} for [Co(hfacac)$_2$(L2)](PF$_6$) at 2 K. the Due to the distortion of the crystal field from the presence of two different ligands and spin-orbit
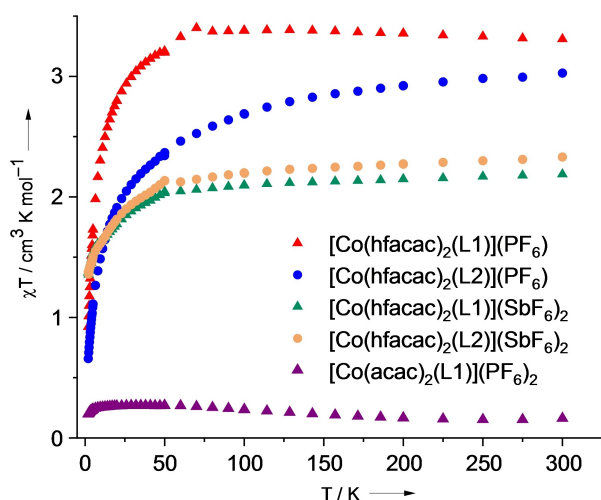
coupling (being large for Co^{II}, for example the spin-orbit coupling constant for the free ion is $\lambda \approx 180$ cm^{-1}[49]), the state with one unpaired electron on Co^{II} is increasingly populated at low temperature.[48,59–61] Antiferromagnetic coupling between the unpaired electron on Co^{II} and the unpaired electron on the guanidine ligand unit in the solid state then leads to a singlet ground state. Due to the various parameters affecting the curve at low temperature (spin-orbit coupling, ligand field, magnetic coupling, and possibly also VT), we abstained from a curve fitting.

For the twofold oxidized complexes [Co(hfacac)$_2$(L1)](SbF$_6$)$_2$ and [Co(hfacac)$_2$(L1)](SbF$_6$)$_2$, χT values of 2.188 cm^3·K·mol^{-1} and 2.331 cm^3·K·mol^{-1}, respectively, were found at 300 K, confirming the presence of high-spin Co^{II} complexes with dicationic ligands. On the other hand, for the analogue acac complex [Co(acac)$_2$(L1)](PF$_6$)$_2$, the χT value measures 0.181 cm^3·K·mol^{-1} at 300 K and slightly increases to 0.276 cm^3·K·mol^{-1} at 40 K, being close to the theoretical value of 0.375 cm^3·K·mol^{-1} obtained from the Curie law for a compound with one unpaired electron (S = $^1/_2$). Hence, the salt [Co(acac)$_2$(L1)](PF$_6$)$_2$ contains a Co^{III} atom and a radical monocationic ligand L1$^{\cdot+}$.

In addition, we recorded magnetometric curves for [Co(acac)$_2$(L3)](PF$_6$)$_2$ and [Co(hfacac)$_2$(L3)](PF$_6$)$_2$ (Figure 13). At 300 K, the χT value is ca. 2.5 cm^3 K mol^{-1} for [Co(acac)$_2$(L3)](PF$_6$)$_2$ and ca. 2.2 cm^3 K mol^{-1} for [Co(hfacac)$_2$(L3)](PF$_6$)$_2$, indicating the presence of a high-spin Co^{II} complex (S = 3/2) with dicationic ligand unit, L3^{2+}. Due to an unquenched orbital contribution in both complexes (^{4}T$_{1g}$ ground term in O$_h$ symmetry), it is higher than the 1.876 cm^3 K mol^{-1} predicted by the Curie law. The χT value drops down below 50 K, reaching eventually 1.1 cm^3 K mol^{-1} at 2 K for [Co(acac)$_2$(L3)](PF$_6$)$_2$ and 0.7 cm^3 K mol^{-1} for [Co(hfacac)$_2$(L3)](PF$_6$)$_2$. The distortion of the crystal field and the spin-orbit coupling remove the degeneracy of the ^{4}T$_{1g}$ ground term. The resulting doublet ground state is increasingly populated at low temperature.[48,59–61] Moreover, a temperature-dependent intramolecular electron-transfer in favor of a radical Co^{III} complex with L3$^{\cdot+}$ at low temperature might occur in [Co(acac)$_2$(L3)](PF$_6$)$_2$, leading to further reduction of the χT value at low temperature. The latter is supported by the observed organic radical signal found in the low temperature (6 K) EPR
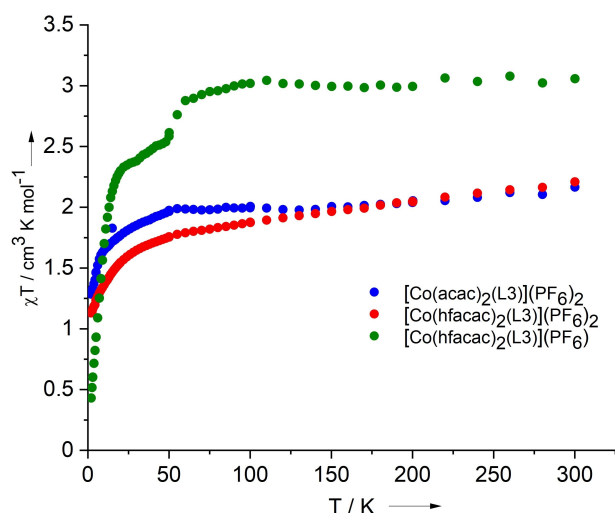

Figure 12. Magnetometric (SQUID) curves for solid [Co(hfacac)$_2$(L1)](PF$_6$), [Co(hfacac)$_2$(L2)](PF$_6$), [Co(hfacac)$_2$(L1)](SbF$_6$)$_2$, [Co(hfacac)$_2$(L2)](SbF$_6$)$_2$ and [Co(acac)$_2$(L1)](PF$_6$)$_2$ at 50 mT.

Chemistry–A European Journal

Full Paper
doi.org/10.1002/chem.202101364

Chemistry Europe
European Chemical
Societies Publishing

Figure 13. Magnetometric (SQUID) curves for solid [Co(acac)$_2$(L3)](PF$_6$)$_2$, [Co(hfacac)$_2$(L3)](PF$_6$) and [Co(hfacac)$_2$(L3)](PF$_6$)$_2$ (all high-spin Co^{II} complexes) at 50 mT.

spectrum of a frozen CH$_2$Cl$_2$ solution and by the quantum-chemical calculations.[43]

A χT value of 3.2 cm^3 K mol^{-1} was measured for [Co(hfacac)$_2$(L3)](PF$_6$) at 300 K, being close to the values obtained for the complexes with L1 and L2 and hfacac co-ligands, and again slightly higher than the 3.001 cm^3 K mol^{-1} predicted by the Curie law for compounds with S = 2. Interestingly, the χT value decreases sharply in the region around 50 K to a value of 2.5 cm^3 K mol^{-1}, before it drops down to 0.43 cm^3 K mol^{-1} at 2 K (Figure 13). Unfortunately, it is not possible to explain unambiguously the behavior around 50 K at this stage, but a spin-crossover (high-spin Co^{II}→low-spin Co^{III}) induced by IET of a part of the complex units could not be excluded; although quantum-chemical calculations on the individual molecules (see below) found a higher energy for the redox isomer with low-spin Co^{III} atom and radical ligand. The low χT value at 2 K could again be explained by an antiferromagnetic coupling between the unpaired electron at the cobalt atom (doublet ground term due to distortion of the crystal field by the different ligands and spin-orbit coupling) and the unpaired electron at the guanidine ligand unit in the solid state. Due to the various parameters that affect the behavior at low temperature (spin-orbit coupling, ligand field, magnetic coupling, possible VT) we again abstained from a curve fitting.

Quantum-chemical calculations

The B3LYP functional together with the def2-TZVP basis set was applied in the calculations. Calculations were carried out without inclusion of the solvent (relative permittivity ε_r of 1), and also with inclusion of a solvent with a relative permittivity ε_r of 37.5 (close to the value of CH$_3$CN), using the conductor-like screening model (COSMO). Of course, it would be desirable to treat such open-shell molecules (e.g. cobalt complexes[30,62]) with multireference methods (such as CASSCF). However, multi-

reference calculations are not simple for molecules of that size. The B3LYP functional was shown previously to give quite reliable results in some cases,[63] including complexes with redox-active guanidines.[43] Moreover, the inclusion of the solvent effect is necessary, in particular for the charged molecules to be dealt with in this work. The main intention of the calculations is not to calculate precisely the electronic properties of individual complexes, but to get estimates of the differences between the electronic properties of the complexes with the related acac and hfacac co-ligands. Therefore, we decided to carry out the calculations with B3LYP/def2-TZVP.

The calculations provide information about the electronic structures and relative energies of the possible redox isomers obtained upon one or two-electron oxidation of the neutral complexes. Tables 6–9 contain some important results of these calculations; in Figure 14 the spin densities are plotted for the

Table 6. Calculated ΔE and ΔG values (B3LYP/def2-TZVP with COSMO) for the redox isomers of the mono- and dicationic complexes with acac co-ligands.

| Monocation[a] | ΔE (quintet–singlet) | | ΔG (quintet–singlet) | |
	$\varepsilon_r = 1$	$\varepsilon_r = 37.5$	$\varepsilon_r = 1$	$\varepsilon_r = 37.5$
[Co(acac)$_2$(L1)]$^+$	−4	+5	−14	−8
[Co(acac)$_2$(L3)]$^+$	−27	−23	−38	−34
dication[a]	ΔE (quartet–doublet)		ΔG (quartet–doublet)	
	$\varepsilon_r = 1$	$\varepsilon_r = 37.5$	$\varepsilon_r = 1$	$\varepsilon_r = 37.5$
[Co(acac)$_2$(L1)]$^{2+}$	+57	+85	+51	+79
[Co(acac)$_2$(L3)]$^{2+}$	+10	−2	+4	−7

[a] Calculations on [Co(acac)$_2$(L2)]$^+$ and [Co(acac)$_2$(L2)]$^{2+}$ failed to converge.

Table 7. Calculated spin populations (B3LYP/def2-TZVP) for the redox isomers of the mono- and dicationic complexes with acac co-ligands (hs = high-spin, ls = low spin, is = intermediate spin).

complex	Co	(hfacac)$_2$	L1/L2/L3	description
[Co(acac)$_2$(L1)]$^+$ (S = 2)	2.735	0.257	1.009	hs-Co^{II}, L1$^{\cdot+}$
[Co(acac)$_2$(L3)]$^+$ (S = 2)	2.735	0.234	1.030	hs-Co^{II}, L3$^{\cdot+}$
[Co(acac)$_2$(L1)]$^{2+}$ (S = 1/2)	0.006	0.012	0.982	ls-Co^{III}, L1$^{\cdot+}$
[Co(acac)$_2$(L1)]$^{2+}$ (S = 3/2)	1.800	0.153	1.047	is-Co^{III}, L1$^{\cdot+}$
[Co(acac)$_2$(L2)]$^{2+}$ (S = 1/2)	0.010	0.009	0.981	ls-Co^{III}, L2$^{\cdot+}$
[Co(acac)$_2$(L3)]$^{2+}$ (S = 1/2)	0.018	0.015	0.966	ls-Co^{III}, L3$^{\cdot+}$
[Co(acac)$_2$(L3)]$^{2+}$ (S = 3/2)	2.720	0.288	−0.008	hs-Co^{II}, L3^{2+}

Table 8. Calculated ΔE and ΔG values (B3LYP/def2-TZVP with COSMO) for the redox isomers of the mono- and dicationic complexes with hfacac co-ligands.

| monocation | ΔE (quintet–singlet) | | ΔG (quintet–singlet) | |
	$\varepsilon_r = 1$	$\varepsilon_r = 37.5$	$\varepsilon_r = 1$	$\varepsilon_r = 37.5$
[Co(hfacac)$_2$(L1)]$^+$	−66	−79	−69	−82
[Co(hfacac)$_2$(L2)]$^+$	−88	−96	−98	−106
[Co(hfacac)$_2$(L3)]$^+$	−72	−81	−78	−87
Dication[a]	ΔE (quartet–doublet)		ΔG (quartet–doublet)	
	$\varepsilon_r = 1$	$\varepsilon_r = 37.5$	$\varepsilon_r = 1$	$\varepsilon_r = 37.5$
[Co(hfacac)$_2$(L1)]$^{2+}$	−17	−51	−32	−65
[Co(hfacac)$_2$(L3)]$^{2+}$	−37	−64	−49	−76

[a] Calculations for [Co(hfacac)$_2$(L2)]$^{2+}$ failed to converge.

Chemistry–A European Journal

Full Paper
doi.org/10.1002/chem.202101364

Chemistry Europe
European Chemical
Societies Publishing

Table 9. Calculated spin populations (B3LYP/def2-TZVP) for the redox isomers of the mono- and dicationic complexes with hfacac co-ligands (hs = high-spin, ls = low spin, is = intermediate spin).

complex	Co	(hfacac)$_2$	L1/L2/L3	description
[Co(hfacac)$_2$(L1)]$^+$ (S=2)	2.719	0.223	1.059	hs-Co^{II}, L1$^{\cdot+}$
[Co(hfacac)$_2$(L2)]$^+$ (S=2)	2.720	0.217	1.063	hs-Co^{II}, L2$^{\cdot+}$
[Co(hfacac)$_2$(L3)]$^+$ (S=2)	2.727	0.215	1.058	hs-Co^{II}, L3$^{\cdot+}$
[Co(hfacac)$_2$(L1)]$^{2+}$ (S=1/2)	0.003	0.010	0.986	ls-Co^{III}, L1$^{\cdot+}$
[Co(hfacac)$_2$(L1)]$^{2+}$ (S=3/2)	2.708	0.258	0.033	hs-Co^{II}, L1^{2+}
[Co(hfacac)$_2$(L2)]$^{2+}$ (S=3/2)	2.708	0.248	0.045	hs-Co^{II}, L2^{2+}
[Co(hfacac)$_2$(L3)]$^{2+}$ (S=1/2)	0.019	0.011	0.971	ls-Co^{III}, L3$^{\cdot+}$
[Co(hfacac)$_2$(L3)]$^{2+}$ (S=3/2)	2.697	0.244	0.058	hs-Co^{II}, L3^{2+}

two redox isomers of [Co(acac)$_2$(L1)]$^+$ and [Co(hfacac)$_2$(L1)]$^+$. For the monocationic complex [Co(acac)$_2$(L1)]$^+$, the redox isomer with S=2 (Co^{II} complex with radical monocationic ligand L1$^{\cdot+}$) is favored by not more than 4 kJ mol^{-1} at ε_r=1 with respect to the diamagnetic redox isomer (S=0, Co^{III} complex with neutral ligand L1). On the other hand, at ε_r=37.5 the diamagnetic redox isomer (S=0) is preferred by 5 kJ mol^{-1}. Due to the higher entropy contribution of the S=2 state (vibrational entropy and entropy from spin (and orbit) degeneracy), ΔG-(quintet – singlet) is negative both at ε_r=1 and 37.5, but still the two redox isomers are close by. The spin density distribution in the redox isomers of [Co(hfacac)$_2$(L1)]$^+$ is similar, but the energy difference is very much different. Here, the S=2 state is clearly favored with ΔE(quintet – singlet) and ΔG-(quintet – singlet) of −66 and −69 kJ mol^{-1}, respectively, at ε_r=1 and −79 and −82 kJ mol^{-1}, respectively, at ε_r=37.5.

Calculations for the S=3/2 state of [Co(acac)$_2$(L1)]$^{2+}$ resulted not in a high-spin Co^{II} complex with dicationic ligand L1^{2+}, but in an intermediate spin Co^{III} complex (Figure 15) with radical monocationic ligand L1$^{\cdot+}$, being energetically disfavored

by 57 kJ mol^{-1} at ε_r=1 and 85 kJ mol^{-1} at ε_r=37.5 with respect to the S=$^1/_2$ state (low-spin Co^{III} with radical monocationic ligand L1$^{\cdot+}$).[43] By contrast, the calculations for [Co(hfacac)$_2$(L1)]$^{2+}$ clearly confirmed the S=3/2 ground state (high-spin Co^{II} complex with dicationic ligand L1^{2+}), being energetically favored by 17 kJ mol^{-1} at ε_r=1 and 51 kJ mol^{-1} at ε_r=37.5 with respect to the S=$^1/_2$ state, in line with the experimental results.

Finally, the electronic structures of the complexes with L3 were analyzed by quantum-chemical calculations; we directly turn to the dicationic complexes. Here, the high-spin Co^{II} redox isomer is stabilized by interligand hydrogen-bonding.[43] For the complex [Co(acac)$_2$(L3)]$^{2+}$, the Co^{III} redox isomer with radical monocationic ligand, L1$^{\cdot+}$, is slightly preferred by 10 kJ mol^{-1} at ε_r=1 with respect to the Co^{II} redox isomer with dicationic ligand, L1^{2+}. On the other hand, it is disfavored by 2 kJ mol^{-1} at ε_r=37.5 (see also the spin density plots in Figure 16). In the corresponding hfacac complex [Co(hfacac)$_2$(L3)]$^{2+}$ the Co^{II} redox isomer is more clearly preferred; by 37 kJ mol^{-1} at ε_r=1 and 64 kJ mol^{-1} at ε_r=37.5.

In the Co^{II} redox isomer of [Co(acac)$_2$(L3)]$^{2+}$ with dicationic ligand, L3^{2+}, the calculated N–H···O hydrogen bond length measures 1.824 Å, being significantly shorter than in the Co^{III} redox isomer with radical monocationic ligand L1$^{\cdot+}$ (2.061 Å). This implies a stabilization of the Co^{II} redox isomer by two strong interligand hydrogen-bonds. For the analogue hfacac complex [Co(hfacac)$_2$(L3)]$^{2+}$, the calculated N–H···O hydrogen bond length measures 1.943/2.114 Å for the redox isomer with dicationic ligand and 2.106/2.375 Å for the redox isomer with radical monocationic ligand, being both significantly longer than in the corresponding acac complexes implying a weaker hydrogen bond. For the two redox isomers of the monocationic complexes of L3, N–H···O hydrogen bond lengths of 1.960/1.814 Å and 2.193/1.895 were found for the diamagnetic Co^{III}
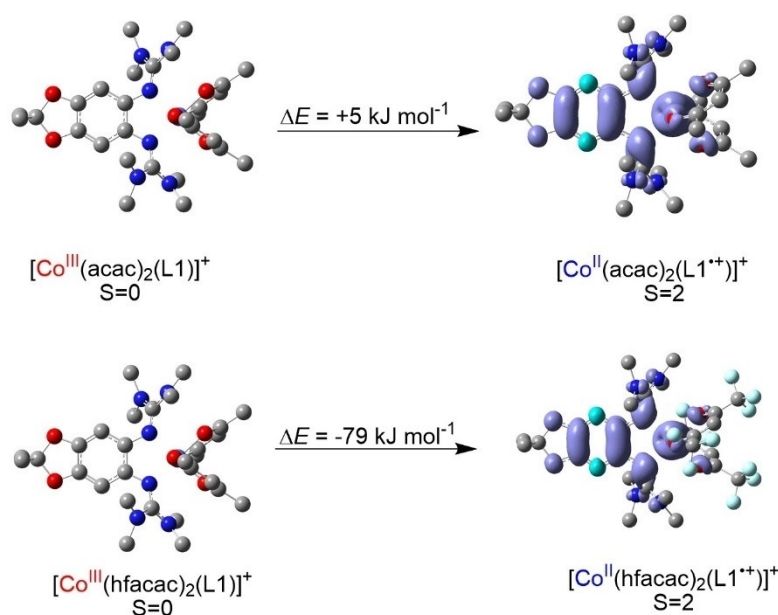

Figure 14. Spin densities and relative energies for the two redox isomers of [Co(acac)$_2$(L1)]$^+$ and [Co(hfacac)$_2$(L1)]$^+$ from B3LYP/def2-TZVP calculations with COSMO (ε_r=37.5). Hydrogen atoms omitted.

Chemistry–A European Journal

Full Paper
doi.org/10.1002/chem.202101364

Chemistry Europe
European Chemical
Societies Publishing

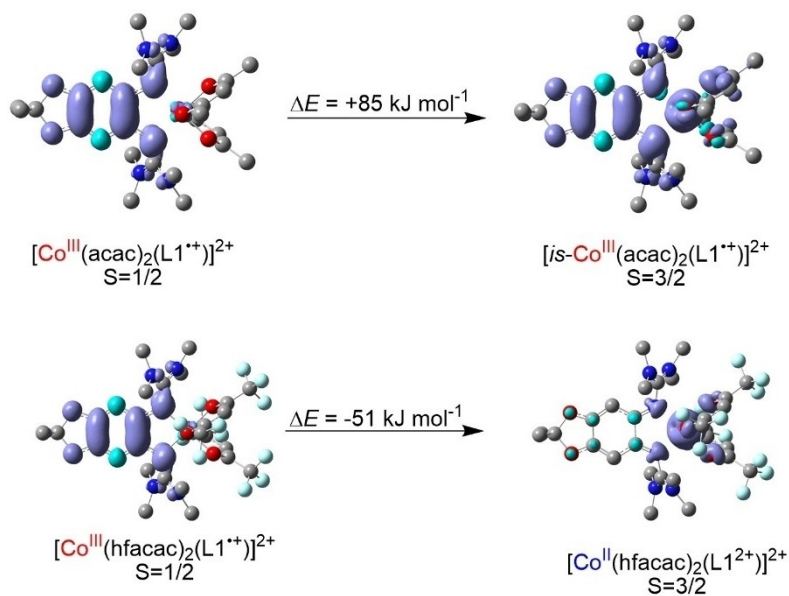**Figure 15.** Spin densities and relative energies for the two redox isomers of $[Co(acac)_2(L1)]^{2+}$ and $[Co(hfacac)_2(L1)]^{2+}$ from B3LYP/def2-TZVP calculations with COSMO ($\varepsilon_r = 37.5$). Hydrogen atoms omitted.

Figure 16. Spin densities and relative energies for the two redox isomers of $[(Co(acac)_2(L3)]^{2+}$ and $[(Co(hfacac)_2(L3)]^{2+}$ from B3LYP/def2-TZVP calculations with COSMO ($\varepsilon_r = 37.5$). Hydrogen atoms omitted.

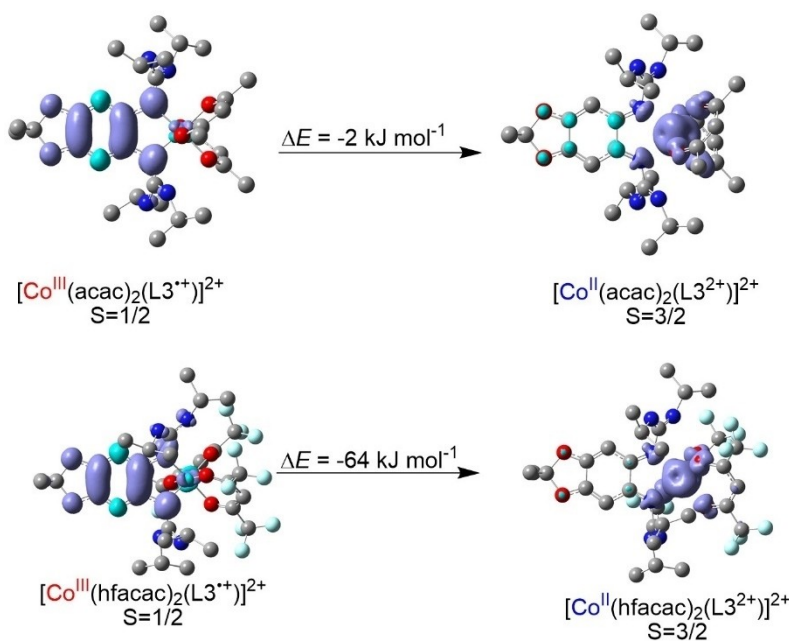isomers of $[Co(acac)_2(L3)]^+$ and $[Co(hfacac)_2(L3)]^+$, respectively, and 1.877 Å and 2.189/1.915 Å for the redox isomer with radical monocationic ligand and Co^{II}, respectively. Again, for both isomers the N–H···O hydrogen bond lengths increase from acac to hfacac co-ligands. A comparison between the more reliable N···O distance within the N–H···O hydrogen bonds of the calculated structures and the crystal structures, confirming the accuracy of the calculations, is found in the Supporting Information. All these calculational results show that hydrogen-bonding is less important for the hfacac complexes.

Conclusions

The detailed understanding and manipulation of the redox chemistry of coordination compounds with redox-active ligands allows their directed use in catalysis and materials science. In

this work, several mononuclear, octahedrally-coordinated cobalt complexes with a redox-active guanidine ligand were synthesized and their redox-chemistry studied. The replacement of the acetylacetonato (acac) co-ligands by the less Lewis basic hexafluoro-acetylacetonato (hfacac) co-ligands leads to a preference for high-spin Co^{II} and destabilization of low-spin Co^{III}. Consequently, chemical one-electron oxidation of the neutral Co^{II} complexes in CH$_2$Cl$_2$ solution leads to Co^{III} complexes with neutral guanidine ligand for complexes with acac co-ligands, but to Co^{II} complexes with radical monocationic guanidine ligand in the case of complexes with hfacac co-ligands. Hence, the simple substitution of the CH$_3$ groups in the co-ligands by CF$_3$ groups changes the electronic structure from a diamagnetic Co^{III} complex (for [Co(acac)$_2$(L1)]$^+$, [Co(acac)$_2$(L2)]$^+$ and [Co(acac)$_2$(L3)]$^+$) to a high-spin Co^{II} complex with four unpaired electrons (for [Co(hfacac)$_2$(L1)]$^+$, [Co(hfacac)$_2$(L2)]$^+$ and [Co(hfacac)$_2$(L3)]$^+$). The ferromagnetic coupling between the two spin centers (Co atom and radical ligand) leads to a significant deviation of the temperature-dependence of the paramagnetic NMR signals from Curie behavior, allowing to experimentally determine the isotropic magnetic exchange coupling constant J in solution. Further one-electron oxidation gives [Co(acac)$_2$(L1)]$^{2+}$ and [Co(acac)$_2$(L2)]$^{2+}$, Co^{III} complexes with radical monocationic ligands. Only for [Co(acac)$_2$(L2)]$^{2+}$, a RIET process induced by the enforcement of the interligand hydrogen bonding upon ligand oxidation leads to a Co^{II} complex with dicationic ligand.[43] By contrast, [Co(hfacac)$_2$(L1)]$^{2+,+}$ [Co(hfacac)$_2$(L2)]^2 and [Co(hfacac)$_2$(L3)]$^{2+}$ all are Co^{II} complexes with dicationic bisguanidine ligands.

The change of the electronic structure evoked by simple co-ligand substitution is accompanied by a massive change in the magnetic and optic properties. The possibility to control these properties in a simple way paves the way for their directed use in various applications. More specifically, the results reported in this work allow the directed synthesis of one out of two possible redox isomers by choice of the co-ligands. They also show that a further fine tuning of the co-ligands is possible. The use of acac ligands in which the methyl groups are replaced by substituents that are less electron-donating than methyl, and less electron-withdrawing than trifluoromethyl, should eventually lead to an adjustment of the energies of the two possible redox isomers of the monocationic complexes. In such cases, both redox isomers are expected to be in equilibrium (valence tautomerism) since the barrier for intramolecular electron transfer (IET) appears to be relatively low in these systems (IET could be triggered by hydrogen-bonding). It will be interesting to see if such equilibria could be obtained both in solution and in the solid state.

Acknowledgements

Conflict of Interest

The authors declare no conflict of interest.

[1] W. I. Dzik, J. I. van der Vlugt, J. N. H. Reek, B. de Bruin, *Angew. Chem.* **2011**, *123*, 3416–3418; *Angew. Chem. Int. Ed.* **2011**, *50*, 3356–3358.
[2] J. I. van der Vlugt, *Eur. J. Inorg. Chem.* **2012**, 363–375.
[3] D. L. J. Broere, R. Plessius, J. I. van der Vlugt, *Chem. Soc. Rev.* **2015**, *44*, 6886–6915.
[4] J. Jacquet, M. Desage-El Murr, L. Fensterbank, *ChemCatChem* **2016**, *8*, 3310–3316.
[5] J. I. van der Vlugt, *Chem. Eur. J.* **2019**, *25*, 2651–2662.
[6] A. Das, Y. Ren, C. Hessin, M. Desage-El Murr, *Beilstein J. Org. Chem.* **2020**, *16*, 858–870.
[7] A. Das, C. Hessin, Y. Ren, M. Desage-El Murr, *Chem. Soc. Rev.* **2020**, *49*, 8840–8867.
[8] T. Tezgerevska, K. G. Alley, C. Boskovic, *Coord. Chem. Rev.* **2014**, *268*, 23–40.
[9] D. N. Hendrickson, C. G. Pierpont, *Top. Curr. Chem.* **2004**, *234*, 63–95.
[10] A. Die, D. Gatteschi, C. Sangregorio, L. Sorace, *Acc. Chem. Res.* **2004**, *37*, 827–835.
[11] E. Evangelio, D. Ruiz-Molina, *Eur. J. Inorg. Chem.* **2005**, 2957–2971.
[12] O. Sato, J. Tao, Y.-Z. Zhang, *Angew. Chem.* **2007**, *119*, 2200–2236; *Angew. Chem. Int. Ed.* **2007**, *46*, 2152–2187.
[13] E. Evangelio, D. Ruiz-Molina, *C. R. Chim.* **2008**, *11*, 1137–1154.
[14] C. Fleming, D. Chung, S. Ponce, D. J. R. Brook, J. DaRos, R. Das, A. Ozarowski, S. A. Stoian, *Chem. Commun.* **2020**, *56*, 4400–4403.
[15] R. M. Buchanan, C. G. Pierpont, *J. Am. Chem. Soc.* **1980**, *102*, 4951–4957.
[16] D. M. Adams, A. Die, A. L. Rheingold, D. N. Hendrickson, *J. Am. Chem. Soc.* **1993**, *115*, 8221–8229.
[17] A. Bencini, A. Caneschi, C. Carbonera, A. Die, D. Gatteschi, R. Righini, C. Sangregorio, J. Van Slageren, *J. Mol. Struct.* **2003**, *656*, 141–154.
[18] J. Tao, H. Maruyama, O. Sato, *J. Am. Chem. Soc.* **2006**, *128*, 1790–1791.
[19] D. M. Adams, B. Li, J. D. Simon, D. N. Hendrickson, *Angew. Chem.* **1995**, *107*, 1580–1582; *Angew. Chem. Int. Ed.* **1995**, *34*, 1481–1483.
[20] D. M. Adams, D. N. Hendrickson, *J. Am. Chem. Soc.* **1996**, *118*, 11515–11528.
[21] P. Gütlich, A. Die, *Angew. Chem.* **1997**, *109*, 2852–2855; *Angew. Chem. Int. Ed.* **1997**, *36*, 2734–2736.
[22] a) O. Sato, S. Hayami, Z.-z. Gu, K. Takahashi, R. Nakajima, K. Seki, A. Fujishima, *J. Photochem. Photobiol. A* **2002**, *149*, 111–114; b) O. Sato, S. Hayami, Z.-z. Gu, K. Takahashi, R. Nakajima, A. Fujishima, *Chem. Phys. Lett.* **2002**, *355*, 169–174.
[23] C. Carbonera, A. Die, J.-F. Létard, C. Sangregorio, L. Sorace, *Angew. Chem.* **2004**, *116*, 3197–3200; *Angew. Chem. Int. Ed.* **2004**, *43*, 3136–3138.
[24] P. Dapporto, A. Die, G. Poneti, L. Sorace, *Chem. Eur. J.* **2008**, *14*, 10915–10918.
[25] C. Roux, D. M. Adams, J. P. Itié, A. Polian, D. N. Hendrickson, M. Verdaguer, *Inorg. Chem.* **1996**, *35*, 2846–2852.
[26] D. Kiriya, H.-C. Chang, S. Kitagawa, *J. Am. Chem. Soc.* **2008**, *130*, 5515–5522.
[27] K. S. Min, A. G. DiPasquale, J. A. Golen, A. L. Rheingold, J. S. Miller, *J. Am. Chem. Soc.* **2007**, *129*, 2360–2368.
[28] J. S. Miller, K. S. Min, *Angew. Chem.* **2009**, *121*, 268–278; *Angew. Chem. Int. Ed.* **2009**, *48*, 262–272.
[29] K. S. Min, A. G. DiPasquale, A. L. Rheingold, H. S. White, J. S. Miller, *J. Am. Chem. Soc.* **2009**, *131*, 6229–6236.
[30] N. P. van Leest, W. Stroek, M. A. Siegler, J. I. van der Vlugt, B. de Bruin, *Inorg. Chem.* **2020**, *59*, 12903–12912.
[31] H.-J. Himmel, *Z. Anorg. Allg. Chem.* **2013**, *639*, 1940–1952.
[32] H.-J. Himmel, *Inorg. Chim. Acta* **2018**, *481*, 56–68.
[33] H.-J. Himmel, *Synlett* **2018**, *29*, 1957–1977.
[34] S. Wiesner, A. Wagner, E. Kaifer, H.-J. Himmel, *Chem. Eur. J.* **2016**, *22*, 10438–10445.
[35] S. Wiesner, A. Wagner, E. Kaifer, H.-J. Himmel, *Dalton Trans.* **2016**, *45*, 15828–15839.
[36] D. F. Schrempp, E. Kaifer, H. Wadepohl, H.-J. Himmel, *Chem. Eur. J.* **2016**, *22*, 16187–16199.

Chemistry–A European Journal

Full Paper
doi.org/10.1002/chem.202101364

Chemistry Europe
European Chemical
Societies Publishing

[37] D. F. Schrempp, E. Kaifer, H.-J. Himmel, *Eur. J. Inorg. Chem.* **2018**, 3660–3667.

[38] D. F. Schrempp, E. Schneider, E. Kaifer, H. Wadepohl, H.-J. Himmel, *Chem. Eur. J.* **2017**, *23*, 11636–11648.

[39] A. Ziesak, T. Wesp, O. Hübner, E. Kaifer, H. Wadepohl, H.-J. Himmel, *Dalton Trans.* **2015**, *44*, 19111–19125.

[40] A. Ziesak, L. Steuer, E. Kaifer, N. Wagner, J. Beck, H. Wadepohl, H.-J. Himmel, *Dalton Trans.* **2018**, *47*, 9430–9441.

[41] S. Haaf, E. Kaifer, H. Wadepohl, H.-J. Himmel, *Chem. Eur. J.* **2021**, 27, 959–970.

[42] F. Schön, E. Kaifer, H.-J. Himmel, *Chem. Eur. J.* **2019**, *25*, 8279–8288.

[43] L. Lohmeyer, F. Schön, E. Kaifer, H.-J. Himmel, *Angew. Chem. Int. Ed.* **2021**, *60*, 10415–10422; *Angew. Chem.* **2021**, *133*, 10506–10514.

[44] D. M. Adams, A. Die, A. L. Rheingold, D. N. Hendrickson, *Angew. Chem.* **1993**, *105*, 954–956.; *Angew. Chem. Int. Ed.* **1993**, *32*, 880–882.

[45] O.-S. Jung, C. G. Pierpont, *Inorg. Chem.* **1994**, *33*, 2227–2235.

[46] U. Wild, C. Neuhäuser, S. Wiesner, E. Kaifer, H. Wadepohl, H.-J. Himmel, *Chem. Eur. J.* **2014**, *20*, 5914–5925.

[47] U. Wild, E. Kaifer, H. Wadepohl, H.-J. Himmel, *Eur. J. Inorg. Chem.* **2015**, 4848–4860.

[48] A. Abragam, M. H. L. Pryce, *Proc. Roy. Soc. A* **1951**, *206*, 173–191.

[49] R. L. Carlin, *Magnetochemistry*, Springer-Verlag Berlin Heidelberg, **1986**.

[50] a) G. N. La Mar, *NMR of Paramagnetic Molecules: Principles and Applications.* Academic Press, INC.: New York and London, **1973**; b) L. Banci, I. Bertini, C. Luchinat, *The ¹H NMR parameters of magnetically coupled dimers – The Fe₂S₂ proteins as an example. In Bioinorganic Chemistry.* Springer Berlin-Heidelberg: Germany, **1990**; Vol. 72, pp 113–136; c) I. Bertini, C. Luchinat, G. Parigi, E. Ravera, *NMR of Paramagnetic Molecules* (Second Edition), Eds.: I. Bertini, C. Luchinat, G. Parigi, E. Ravera, Elsevier, Boston, **2017**; d) H. Liimatainen, T. O. Pennanen, J. Vaara, *J. Can. J. Chem.* **2009**, *87*, 954–964; e) M. Enders, *Assigning and Understanding NMR Shifts of Paramagnetic Metal Complexes. In Modeling of Molecular Properties*, P. Comba, Ed; Wiley-VCH: Weinheim, Germany, **2011**.

[51] a) H. Hilbig, P. Hudeczek, F. H. Köhler, X. Xie, P. Bergerat, O. Kahn, *Inorg. Chem.* **1998**, *37*, 4246–4257; b) D. L. Reger, A. E. Pascui, P. J. Pellechia, A. Ozarowski, *Inorg. Chem.* **2013**, *52*, 12741–12748; c) P. W. Kopf, R. W. Kreilick, *J. Am. Chem. Soc.* **1969**, *91*, 6569–6573; d) M. Damjanović, T. Morita, K. Katoh, M. Yamashita, M. Enders, *Chem. Eur. J.* **2015**, *21*,

14421–14432; e) T. E. Machonkin, W. M. Westler, J. L. Markley, *Inorg. Chem.* **2005**, *44*, 779–797.

[52] P. Roquette, A. Maronna, M. Reinmuth, E. Kaifer, M. Enders, H.-J. Himmel, *Inorg. Chem.* **2011**, *50*, 1942–1955.

[53] A. Maronna, O. Hübner, M. Enders, E. Kaifer, H.-J. Himmel, *Chem. Eur. J.* **2013**, *19*, 8958–8977.

[54] B. Eberle, M. Damjanovic, M. Enders, S. Leingang, J. Pfisterer, C. Krämer, O. Hübner, E. Kaifer, H.-J. Himmel, *Inorg. Chem.* **2016**, *55*, 1683–1696.

[55] P. Roquette, A. Maronna, A. Peters, E. Kaifer, H.-J. Himmel, Ch. Hauf, V. Herz, E.-W. Scheidt, W. Scherer, *Chem. Eur. J.* **2010**, *16*, 1336–1350.

[56] Deposition Numbers 2077274 (for [Co(hfacac)₂(L1)]), 2077273 (for [Co(hfacac)₂(L2)]), 2077278 (for [Co(hfacac)₂(L3)]), 2077275 (for [Co(hfacac)₂(L1)](PF₆)), 2077276 (for [Co(hfacac)₂(L2)](PF₆)), and 2077277 (for [Co(hfacac)₂(L3)](PF₆)) contain the supplementary crystallographic data for this paper. These data are provided free of charge by the joint Cambridge Crystallographic Data Centre and Fachinformationszentrum Karlsruhe Access Structures servicewww.ccdc.cam.ac.uk/structures.

[57] S. N. Brown, *Inorg. Chem.* **2012**, *51*, 1251–1260.

[58] F. J. de Zwart, B. Reus, A. A. H. Laporte, V. Sinha, B. de Bruin, *Inorg. Chem.* **2021**, *60*, 3274–3281.

[59] H. Jankovics, M. Daskalakis, C. P. Raptopoulou, A. Terzis, V. Tangoulis, J. Giapintzakis, T. Kiss, A. Salifoglou, *Inorg. Chem.* **2002**, *41*, 3366–3374.

[60] A. Rodriguez, H. Sakiyama, N. Masciocchi, S. Galli, N. Gálvez, F. Lloret, E. Colacio, *Inorg. Chem.* **2005**, *44*, 8399–8406.

[61] F. Lloret, M. Julve, J. Cano, R. Ruiz-Garcia, E. Pardo, *Inorg. Chim. Acta* **2008**, *361*, 3432–3445.

[62] See, for example, the discussion in: N. P. van Leest, M. A. Tepaske, J.-P. H. Oudsen, B. Venderbosch, N. R. Rietdijk, M. A. Siegler, M. Tromp, J. I. van der Vlugt, B. de Bruin, *J. Am. Chem. Soc.* **2020**, *142*, 552–563.

[63] See, for example: D. L. J. Broere, N. P. van Leest, B. de Bruin, M. A. Siegler, J. I. van der Vlugt, *Inorg. Chem.* **2016**, *55*, 8603–8611.